



Structural topology optimization for frequency response problem using model reduction schemes[☆]

Gil Ho Yoon

School of Mechanical Engineering, Kyungpook National University, Republic of Korea

ARTICLE INFO

Article history:

Received 13 October 2009

Received in revised form 3 February 2010

Accepted 7 February 2010

Available online 1 March 2010

Keywords:

Topology optimization

Model reduction method

Ritz vector method

Mode superposition method

Quasi-static Ritz vector method

ABSTRACT

This study uses model reduction (MR) schemes such as the mode superposition (MS), Ritz vector (RV), and quasi-static Ritz vector (QSRV) methods, which reduce the size of the dynamic stiffness matrix of dynamic structures, to calculate dynamic responses and sensitivity values with adequate efficiency and accuracy for topology optimization in the frequency domain. The calculation of structural responses to dynamic excitation using the framework of the finite element (FE) procedure usually requires a significant amount of computation time; that is mainly attributable to repeated inversions of dynamic stiffness matrices depending on time or frequency intervals, which hastens the dissemination of the MR schemes in the analysis. However, using well-established MR schemes in topology optimization has not been prevalent. Therefore, this study conducted a comprehensive investigation to highlight the drawbacks and advantages of these MR schemes for topology optimization. In the results, the MS method, which generates reduction bases by considering some of the lowest eigenmodes, can lose the accuracy in both approximated structural responses and sensitivity values due to locally vibrating eigenmodes and higher mode truncation in the solid isotropic material with penalization (SIMP) approach. In addition, the RV and QSRV methods, which generate reduction bases by considering the external force, mass, and stiffness matrices of a structure, can be used as alternative model reduction schemes for stable optimization. Through several analysis and design examples, the efficiency and reliability of the model reduction schemes for topology optimization are compared and validated.

© 2010 Elsevier B.V. All rights reserved.

1. Introduction

Improving of the vibration or noise characteristics of a structure by changing its geometry has long been a subject that has fascinated the minds of engineers and scientists [1–12]. In order to improve these characteristics systematically by using the finite element (FE) procedure, so-called size and shape optimizations, which modify the size and shape parameters of a structure through mathematical programming, have been developed and applied to various engineering structures. Moreover, the topology inside a design domain can be changed without a given initial topology by using the topology optimization scheme; the basic idea is that the material properties of each element are interpolated from those of nonstructural domain (hereinafter called “Void”) and to those of structural domain (hereinafter called “Solid”) with respect to the design variable defined on each element. Depending on how the material properties are modeled with respect to the design variable, the solid isotropic material with penalization (SIMP) approach or the homogenization-based approach can be used [1]. Recently the element connectivity based parameterization method has also been used [13,14].

In this study, we investigated how the vibration (or noise) characteristics of structure can be efficiently improved on the basis of the

approximated structural frequency response function (FRF). Initial researches on FRF optimization including sensitivity analysis was published in the early 1970s (see [15,16]). In topology optimization, Ma et al. applied the mode superposition (MS) scheme to a dynamic compliance minimization problem within the framework of the homogenization-based approach and developed the modified optimality criteria (OC) algorithm for convex optimization [17]. Diaz and Kikuchi applied topology optimization by considering the eigenvalues of a structure for optimal plate reinforcement [5]. After these researches, Jog reintroduced the concept of the dynamic compliance and made the important physical observation that a structure similar to the static compliance minimization problem can be obtained by minimizing the dynamic compliance of a low frequency domain in linear structures; this was later validated for acoustic-structure interaction problem and nonlinear dynamic problem as well [4,17]. Tcherniak applied topology optimization to design resonating structures [18] and Kim and Kim and Maeda et al. designed vibrating structures with specified eigenfrequencies and eigenmode shape [10,12]. During structural optimization of dynamic problem, it is also important to consider multiple eigenfrequencies. Because the eigenvectors of the repeated eigenvalues cannot be calculated uniquely, the sensitivity analysis of these eigenfrequencies becomes complicated [19].

Although topology optimization for dynamic structures is of interest, the very high computation time required for the optimization often becomes a problem in practical applications [20–22]. In particular,

[☆] This research was supported by Basic Science Research Program through the National Research Foundation of Korea (NRF) funded by the Ministry of Education, Science and Technology (2009-0087705).

E-mail addresses: ghy@knu.ac.kr, gilho.yoon@gmail.com.

when we consider topology optimization for complex manifold structures with fine incremental times or frequencies, a lot of FE calls to dynamic response analysis apparently result in a large computation time. A popular remedy to reduce the computation time in the FE procedure is to reduce the system size prior to calculating the structural responses by using the model reduction schemes (MR schemes) such as the Guyan reduction method, the mode superposition method (MS method), the Ritz vector method (RV method), and the Quasi-static Ritz vector method (QSRV method). To the best of our knowledge, Ma et al. (1993) were the first to introduce the MS method within the framework of the homogenization-based topology optimization; they discussed the representation error of the original FRF using the MS method [7]. Later Jacob employed the Pade approximation method and demonstrated its advantages in structural and acoustic topology problems [23].

In the study, we first investigated the MS method for evaluating FRFs in the framework of the SIMP-based topology optimization, which can be regarded as an extension of Ma et al.'s work in which the homogenization-based material interpolation was employed [7]. And here it is a newly found insight that owing to the differences in the design variables and the associated ratio differences of the stiffness to the mass stiffness matrices of the SIMP and the homogenization-based approaches, the MS method can often fail to provide optimal layouts based on reasonably approximated structural responses in the framework of the SIMP approach. By investigating these failures in detail, it is one of our findings that the highly localized eigen modes, which are locally vibrating modes around finite elements with weak Young's moduli, and the higher mode truncation cause the approximated solution obtained by using the MS method to become seriously inaccurate [10,17,24,25]. To overcome this side effect of the MS method, the RV method and QSRV methods were implemented in the framework of the SIMP approach; these methods reduce the size of the dynamic stiffness matrix by considering the boundary condition and the mass and stiffness of the systems and are also popular reduction methods for the FE procedure. Because the localized vibration modes of the MR scheme were not observed in these two MR schemes, we found that they can provide more accurate and efficient reduced models in the framework of the SIMP approach. We present several numerical examples to compare these three MR schemes in this paper.

The layout of the paper is as follows. After describing the density-based topology optimization formulation for dynamic problems, we introduce and implement some MR schemes in the framework of the SIMP approach. The RV method and the QSRV methods are newly introduced for topology optimization. Using some analysis benchmark examples in which the material properties and boundary conditions are arbitrarily chosen, the efficiency and characteristics of the discussed MR schemes are numerically studied and compared with regard to topology optimization. Some numerical issues pertaining to the MS method owing to the locally vibrating modes, which creates problematic in the density-based topology optimization for eigenfrequencies and self-loading, are newly found with regard to dynamic response optimization [1,9–11,25]. A wave transmit design problem that requires the solution of an adjoint problem formulated by the structural response approximated by the MR schemes is considered. Finally, our findings and some topics for future research are summarized and discussed in the conclusion.

2. Statement of optimization formulation

2.1. Basic FE procedure for linear structural analysis

In many cases of practical interest, the linear structural response of a structure with the time varying force \mathbf{F}_t is formulated by Newton's law as follows.

$$\mathbf{M}\ddot{\mathbf{X}}_t + \mathbf{C}\dot{\mathbf{X}}_t + \mathbf{K}\mathbf{X}_t = \mathbf{F}_t \quad (1)$$

where \mathbf{M} , \mathbf{C} , and \mathbf{K} represent the mass matrix, damping matrix and stiffness matrices, respectively. The time varying displacement, velocity, and acceleration of a structure are denoted by \mathbf{X}_t , $\dot{\mathbf{X}}_t$, and $\ddot{\mathbf{X}}_t$ with the right subscript t , respectively. In this study, because the studying nonlinear structures and boundary conditions is too involved a subject to be discussed in detail, \mathbf{M} , \mathbf{C} , and \mathbf{K} are assumed to be independent to structural displacements. In general, the finite element procedure is used to formulate the linear stiffness matrix, mass matrix and damping matrices.

$$\mathbf{M} = \sum_{e=1}^{NE} \mathbf{m}_e, \quad \mathbf{K} = \sum_{e=1}^{NE} \mathbf{k}_e \quad (2)$$

$$\mathbf{m}_e = \int_{\Omega_e} \rho \mathbf{H}^T \mathbf{H} d\Omega, \quad \mathbf{k}_e = \int_{\Omega_e} \mathbf{B}^T \mathbf{D} \mathbf{B} d\Omega \quad (3)$$

$$\mathbf{C} = \alpha_r \mathbf{M} + \beta_r \mathbf{M} \quad (4)$$

where the total number of elements is NE . The stiffness and mass matrices of the e -th element with the domain Ω_e are \mathbf{k}_e and \mathbf{m}_e , respectively. The shape function and the strain-displacement matrices are denoted by \mathbf{H} and \mathbf{B} , respectively. The structural density (mass density) of the e -th element and the homogeneous constitutive matrix inside elements are ρ and \mathbf{D} , respectively. For the sake of simplicity, the Rayleigh damping was assumed with the damping coefficients α_r and β_r from Eq. (4).¹ Furthermore, appropriate boundary conditions must be inserted to the linear momentum balance Eq. (1).

To obtain the structural displacements with the harmonic loading ω at a certain excitation frequency, the force \mathbf{F}_t and the displacement \mathbf{X}_t are assumed to vary harmonically as follows.

$$\mathbf{X}_t = \mathbf{X}e^{i\omega t}, \quad \mathbf{F}_t = \mathbf{F}e^{i\omega t} \quad (5)$$

Here, the amplitudes of the complex structural displacement and complex force are denoted by \mathbf{X} and \mathbf{F} without the subscript t to avoid confusion with the time varying displacement and force \mathbf{X}_t and \mathbf{F}_t , respectively. The substitution of Eq. (5) in Eq. (1) yields

$$[-\omega^2 \mathbf{M} + i\omega \mathbf{C} + \mathbf{K}]\mathbf{X} = \mathbf{F} \quad (6)$$

$$\mathbf{S} = [-\omega^2 \mathbf{M} + i\omega \mathbf{C} + \mathbf{K}] \quad (7)$$

where the dynamic stiffness matrix is defined as \mathbf{S} [21].

2.2. Statement of topology optimization formulation

2.2.1. Dynamic compliance minimization problem

The design of stiff structures for given static or dynamic loads has been an important issue in many structural applications. For static and quasi-static structures, stiff structures can be obtained by means of minimizing the static compliance, which is defined as the inner product of the external force and static (or quasi-static) displacements. However, for dynamic structures with time-varying forces and displacements, defining and establishing a measure for dynamic stiffness are required. Based on several important discussions made in the references [4,5,7,8,16,17], a dynamic compliance measure defined in the frequency domain has recently been introduced for topology optimization; this subject should be researched further, but this subject is too complicated to be discussed here. For the sake of simplicity,

¹ Many studies elaborating on the model reduction (MR) schemes for unconventional damping exist. However, this study simplifies the damping model to the Rayleigh damping model for application to topology optimization.

the following dynamic compliance definition provided by Ma et al. [7] and Jacob [23] is employed in this study.

$$\Phi = \int_{\omega_s}^{\omega_e} |\mathbf{F}^T \mathbf{X}| d\omega \quad (8)$$

$$= \int_{\omega_s}^{\omega_e} \sqrt{(\mathbf{F}^T \mathbf{X}_{real})^2 + (\mathbf{F}^T \mathbf{X}_{imag})^2} d\omega$$

where the starting and ending angular speeds are denoted by ω_s and ω_e , respectively. The real and imaginary parts of the structural displacements are defined by X_{real} and X_{imag} , respectively.

For topology optimization based on the SIMP approach with a penalty n , the Young's modulus and the structural density (mass density) are interpolated as follows.

$$E(\gamma) = E_0 \gamma^n \quad (9)$$

$$\rho(\gamma) = \rho_0 \gamma \quad (10)$$

$$0.001 = \gamma_{min} \leq \gamma \leq 1. \quad (11)$$

The nominal Young's modulus and the structural density are E_0 and ρ_0 , respectively. The design variable γ is varying from a very small number, γ_{min} , to 1. Depending on the SIMP penalty n , weak Young's moduli for void areas are determined, i.e., $10^{-9}E_0$ with 3 for n and $10^{-12}E_0$ with 4 for n .

Topology optimization of a linear problem minimizing the dynamic compliance of Eq. (8) subject to the mass constraint is formulated as follows.

$$\begin{aligned} \text{Min}_{\gamma} \quad & \Phi = \int_{\omega_s}^{\omega_e} |\mathbf{F}^T \mathbf{X}| d\omega \\ \text{s.t.} \quad & \sum_{e=1}^{NE} \rho_e(\gamma_e) V_e \leq V^* \end{aligned} \quad (12)$$

where the volume of the e -th element and the prescribed volume limit are V_e and V^* , respectively.

To solve the optimization formulation (12), a mathematical optimization algorithm, which is the method of moving asymptotes, is employed here [26]. Furthermore, the sensitivity analysis for the object function and the constraint with respect to the design variable γ should be derived. By adopting the adjoint variable method (AVM), the following sensitivity analysis can be derived from the Eq. (8).

$$\phi_L = \phi(\omega) + \lambda_1^T (\mathbf{S} \mathbf{X} - \mathbf{F}) + \lambda_2^T (\bar{\mathbf{S}} \bar{\mathbf{X}} - \bar{\mathbf{F}}) \quad \text{where } \phi = |\mathbf{F}^T \mathbf{X}| \quad (13)$$

where the conjugate dynamic stiffness and the conjugate force are $\bar{\mathbf{S}}$ and $\bar{\mathbf{F}}$, respectively. The lagrangian multipliers are λ_1 and λ_2 . By differentiating the Lagrangian equation ϕ_L , the following sensitivity analysis and two adjoint variables, λ_1 and λ_2 , can be obtained.

$$\frac{d\phi_L}{d\gamma} = \frac{\partial \phi}{\partial \gamma} + \lambda_1^T \left(\frac{\partial \mathbf{S}}{\partial \gamma} \mathbf{X} - \frac{\partial \mathbf{F}}{\partial \gamma} \right) + \lambda_2^T \left(\frac{\partial \bar{\mathbf{S}}}{\partial \gamma} \bar{\mathbf{X}} - \frac{\partial \bar{\mathbf{F}}}{\partial \gamma} \right) \quad (14)$$

$$\mathbf{S} \lambda_1 = \frac{1}{2} \left(-\frac{\partial \phi}{\partial \mathbf{X}_{real}} + i \frac{\partial \phi}{\partial \mathbf{X}_{imag}} \right) \quad (15)$$

$$\bar{\mathbf{S}} \lambda_2 = \frac{1}{2} \left(-\frac{\partial \phi}{\partial \mathbf{X}_{imag}} - i \frac{\partial \phi}{\partial \mathbf{X}_{real}} \right) \text{ or } \left(\mathbf{S} \bar{\lambda}_2 = \frac{1}{2} \left(-\frac{\partial \phi}{\partial \mathbf{X}_{imag}} + i \frac{\partial \phi}{\partial \mathbf{X}_{real}} \right) \right) \quad (16)$$

By comparing the conjugate of the Eq. (16) with the Eq. (15), we can know that $\lambda_1 = \bar{\lambda}_2$. Therefore the following equation can be obtained.

$$\frac{d\phi_L}{d\gamma} = \frac{\partial \phi}{\partial \gamma} + 2 \times \text{Real} \left(\lambda^T \left(\frac{\partial \mathbf{S}}{\partial \gamma} \mathbf{X} - \frac{\partial \mathbf{F}}{\partial \gamma} \right) \right) \quad (17)$$

$$\mathbf{S} \lambda = -\frac{1}{2} \left(\frac{\partial \phi}{\partial \mathbf{X}_{real}} - i \frac{\partial \phi}{\partial \mathbf{X}_{imag}} \right) \quad (18)$$

As a final formulation, the following sensitivity value integrated over a frequency domain can be obtained.

$$\frac{d\Phi}{d\gamma} = \int_{\omega_s}^{\omega_e} 2 \text{Real} \left(\lambda^T \frac{d\mathbf{S}}{d\gamma} \mathbf{X} \right) d\omega \quad (19)$$

$$\lambda = \frac{-\alpha}{2} \mathbf{X}, \alpha = \frac{\mathbf{X}^T \mathbf{F}}{|\mathbf{X}^T \mathbf{F}|} \quad (20)$$

2.2.2. Reinforcement design of two-dimensional actuation mechanism

As another example, the following force excitation problem, which is a nonself-adjoint problem, is considered.

$$\Phi = \int_{\omega_s}^{\omega_e} |\mathbf{X} \mathbf{L} \bar{\mathbf{X}}| d\omega \quad (21)$$

where the matrix \mathbf{L} can be defined as a $n \times n$ matrix dependent on the chosen measurements. For the sensitivity analysis, the following equations are used.

$$\mathbf{S} \lambda = -\mathbf{L} \bar{\mathbf{X}} \quad (22)$$

$$\frac{d\Phi}{d\gamma} = \int_{\omega_s}^{\omega_e} 2 \text{Real} \left(\lambda^T \frac{d\mathbf{S}}{d\gamma} \mathbf{X} \right) d\omega \quad (23)$$

It should be noted that the adjoint variables λ is solved by the Eq. (22) with the force vector, $-\mathbf{L} \bar{\mathbf{X}}$, which is itself a function of \mathbf{X} . Therefore, using the MR schemes, the force term, $-\mathbf{L} \bar{\mathbf{X}}$, as well as the dynamic stiffness matrix \mathbf{S} are approximated; consequently, the accuracy of the sensitivity analysis decreases than that of the structural response.

3. Solutions in the framework of the model reduction scheme (MR scheme) for topology optimization

3.1. Introduction to the model reduction scheme (MR scheme)

FE analysis when evaluating the responses of a structure to dynamic loadings is important and fundamental to computational structural dynamics. To calculate structural responses accurately, the number of degrees of freedom in computational FE models has been dramatically increased with the help of the development of advanced computers and algorithms. However, even the most advanced and best cultured computers and algorithms once come to their limit when only the MR scheme helps. In other words, it is often advantageous and sometimes necessary to transform a set of the system equations of complex FE model into a set of reduced equations with a smaller number of degrees of freedom; the accuracy is inevitably affected, but the reduced accuracy is adequate from an engineering standpoint. It should be noted that the use of the MR scheme does not imply modeling the considered structure with a small number of elements and nodes (coarse discretized FE mesh) rather it implies transforming the global dynamic stiffness matrix of highly refined FE meshes into a smaller matrix (reduced dynamic stiffness matrix) by changing the geometric or nodal coordinates of the refined FE mesh into the so-called generalized or modal coordinates, which are explained in the later of this section [21,22]. Numerical characteristics such as the computation time, solution accuracy, and sparsity of the reduced dynamic stiffness matrix are highly dependent on the characteristics of the employed reduction bases.

As stated above, most existing research on the MR schemes has been geared towards finding efficient reduction bases for dynamic structures. Depending on the characteristics of the dynamic structures

being considered in defining these reduction bases, various reduction schemes are available, such as the Guyan reduction, mode superposition (MS), Ritz vector (RV), modal acceleration, and quasi-static Ritz vector (QSRV) methods [7,20–22,27–30]. Despite differences in their reduction bases, the ultimate and common goal of these methods is the reduction of the number of degrees of freedom for computational efficiency. A research published by R. J. Guyan in 1964 stated reduced stiffness and mass matrices based on the static condensation of unwanted or dependent coordinates is the first major step toward realizing a method of reducing the size of the system equation of a dynamic structure [15,20]. The other methods transform a large number of system equations into a small number of equations by approximating the original structural response to the approximated response, $\Psi\mathbf{Q}$, by changing the orthogonal bases in the standard coordinates to the user-chosen modal bases. (See [21,22] for the mathematical definitions.) Mathematically, the approximated response, \mathbf{X}_A , of the original response \mathbf{X} can be written as follows:

$$\mathbf{X} \approx \mathbf{X}_A = \Psi\mathbf{Q} \quad (24)$$

$$\Psi = [\varphi_1, \varphi_2, \dots, \varphi_{n_d}] \quad (n_d \leq n) \quad (25)$$

where Ψ is the retained set of the considered orthonormal basis φ_i and \mathbf{Q} is the time or frequency dependent vector of the order n_d . If arbitrary n bases orthonormal to each other are chosen for φ_i , it is possible in principle to exactly calculate the original responses of dynamic structures by substituting Eq. (24) into Eq. (6).

By pre-multiplying Ψ^T into the dynamic equation, the following reduced equation with the order n_d is obtained.

$$\underbrace{\{\Psi^T[-\omega^2\mathbf{M} + i\omega\mathbf{C} + \mathbf{K}]\Psi\}}_{n_d \times n_d} \underbrace{\mathbf{Q}}_{n_d \times 1} = \underbrace{\Psi^T\mathbf{F}}_{n_d \times 1} \quad (26)$$

By solving the above reduced system, the approximated frequency solution \mathbf{X}_A is obtained. Here it could be interpreted that new stiffness, mass, and damping matrices are constructed. While not explicitly explained, the above expressions are also applicable to the time domain. In MR schemes, we commonly use a small number of bases ($n_d \ll n$) that results in approximated frequency responses; now, the issue becomes how to properly choose φ_i and n_d to produce reasonably accurate responses from an engineering point of view. Therefore, depending on the choice of Ψ for different engineering purposes, a number of schemes have been developed.

3.2. The mode superposition method (MS method)

The MS method calculates the reduction bases, Ψ , of Eq. (25) by calculating the eigenmodes of the original dynamic structures [7,21,22]. To reduce the order of the governing Eq. (1), several lowest eigenvalues are selected depending on the frequency domains of interest. In principle, if all eigenmodes of a dynamic structure are chosen for the bases Ψ , the calculated response of the transformed Eq. (26) becomes the same as the dynamic response of the original system Eq. (6); however, due to the accumulated round-off error, especially when calculating eigenvalues and associated eigenmodes, additional errors of the approximated responses to the original response is inevitably introduced, even with all the eigenmodes in practice.

To start with, the standard eigenvalue problem of the original FE model with a mass stiffness matrix, \mathbf{M} , and a stiffness matrix, \mathbf{K} , is solved for the j -th eigenvalues ω_j and the associate j -th eigenmodes φ_j ($j = 1, \dots, n_d$).

$$\varphi_j^T [\mathbf{K} - \omega_j^2 \mathbf{M}] \varphi_j = 0 \quad (j = 1 \dots n_d, n_d \leq n, \text{Rank}(\mathbf{M}) = \text{Rank}(\mathbf{K}) = n) \quad (27)$$

$$\omega_1 \leq \omega_2 \leq \dots \leq \omega_{n_d-1} \leq \omega_{n_d}. \quad (28)$$

Using the retained n_d bases, the transformation matrix Ψ can be defined as shown in Eq. (29). It turns out that $\Psi^T\mathbf{M}\Psi$ becomes the identity matrix with size $n_d(\mathbf{I}_{n_d \times n_d})$ whereas the main diagonal values and off-diagonal values of $\Psi^T\mathbf{K}\Psi$ are the vibration frequencies squared (ω_j^2) and zeros, respectively. The Rayleigh damping matrix is also decomposed into Eq. (32) when using the MS method.

$$\text{MS method: } \Psi = [\varphi_1, \varphi_2, \dots, \varphi_{n_d}] \quad (29)$$

$$\Psi^T\mathbf{M}\Psi = \mathbf{I}_{n_d \times n_d} \quad (30)$$

$$\Psi^T\mathbf{K}\Psi = \begin{bmatrix} \omega_1^2 & \dots & 0 \\ \vdots & \ddots & \vdots \\ 0 & 0 & \omega_{n_d}^2 \end{bmatrix} \quad (31)$$

$$\Psi^T\mathbf{C}\Psi = \alpha_r \mathbf{I}_{n_d \times n_d} + \beta_r \begin{bmatrix} \omega_1^2 & \dots & 0 \\ \vdots & \ddots & \vdots \\ 0 & 0 & \omega_{n_d}^2 \end{bmatrix} \quad (32)$$

The structural response \mathbf{X} for the excitation frequency ω can then be obtained by solving the algebraic Eq. (33).

$$\mathbf{X} \approx \mathbf{X}_A = \sum_{e=1}^{n_d} q_e \varphi_e, q_e = \frac{\varphi_e^T \mathbf{F}}{\omega_e^2 - \omega^2 + (\alpha_r + \beta_r \omega_e^2) i} \quad (33)$$

It should be noted that the response of Eq. (33) is obtained by solving uncoupled linear equations with one unknown without applying Gauss's elimination of the dynamic stiffness matrix. The popularity of the MS method can be attributed to its simplicity and accuracy, and it is regarded as a standard with plenty of researches being carried out to study its applications in dynamic analysis. Furthermore, almost all commercial software such as ANSYS, NASTRAN, and ABAQUS implement the MS method as a basic option. In topology optimization, the MS method was firstly studied by Ma et al. for a dynamic system equation without the damping matrix in the framework of the homogenization based topology optimization [7].

3.3. The Ritz vector method (RV method)

As an alternative to the MS method, the Ritz vector method constructs its reduction bases Ψ by considering the external force \mathbf{F} , mass matrix \mathbf{M} , and stiffness matrix \mathbf{K} [15,21,22,27,28]. In the RV method, the first basis, φ_1 , is constructed by solving the static equation and normalizing the static displacement to the mass matrix as follows.

$$\varphi_1 = \frac{1}{\varphi_1^T \mathbf{M} \varphi_1} \varphi_1^*, \quad \varphi_1^* \equiv \mathbf{K}^{-1} \mathbf{F}. \quad (34)$$

The next bases are sequentially constructed by considering the mass and stiffness matrices of a dynamic system, whereas the previously calculated bases are used to make a new basis orthogonal to them.

$$\varphi_j^* \equiv \mathbf{K}^{-1} (\mathbf{M} \varphi_{j-1}) \quad (35)$$

$$\text{Orthogonalization: } \varphi_j^{**} \equiv \varphi_j^* - \sum_{k=1}^{j-1} (\varphi_k^{*T} \mathbf{M} \varphi_k^*) \varphi_k \quad (36)$$

$$\text{Normalization: } \varphi_j = \frac{1}{\varphi_j^{**T} \mathbf{M} \varphi_j^{**}} \varphi_j^{**} \quad (37)$$

where φ_j with the right superscript (*) and (**) denote auxiliary variables. In the Eq. (35), the LU (or LDU) decomposition method writes the stiffness matrix as the product of a lower and an upper

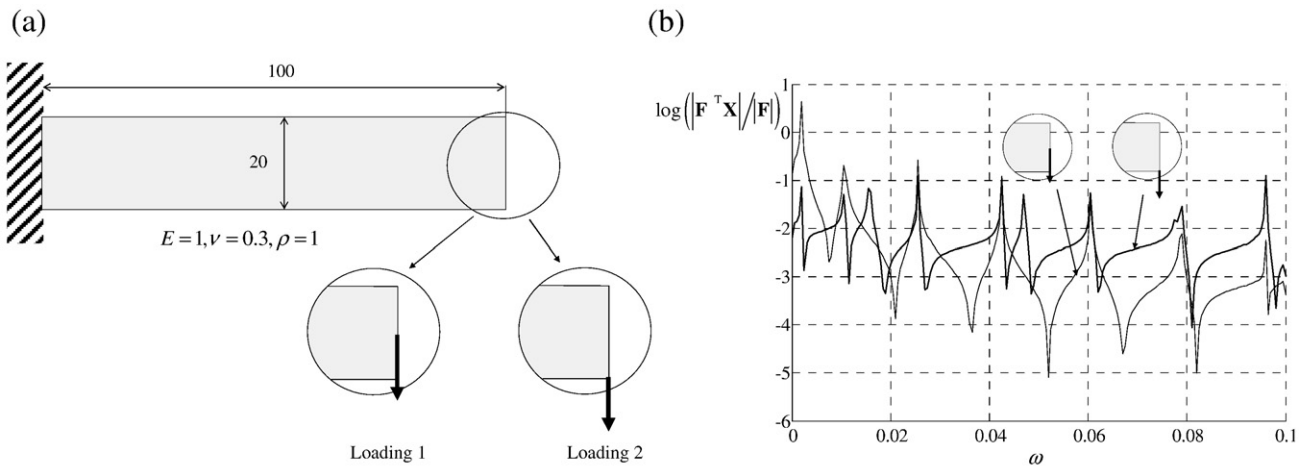


Fig. 1. Analysis example. (a) Problem definition and (b) FRFs with two different forces.

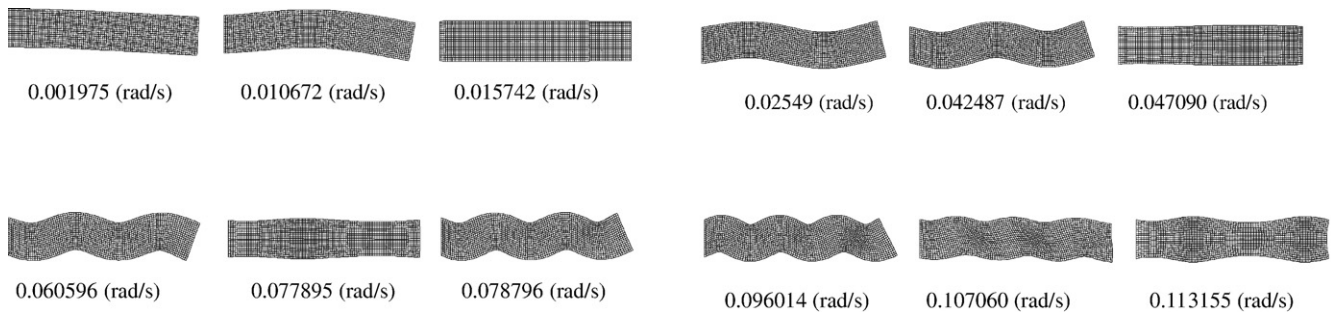


Fig. 2. Eigenmodes of the structure.

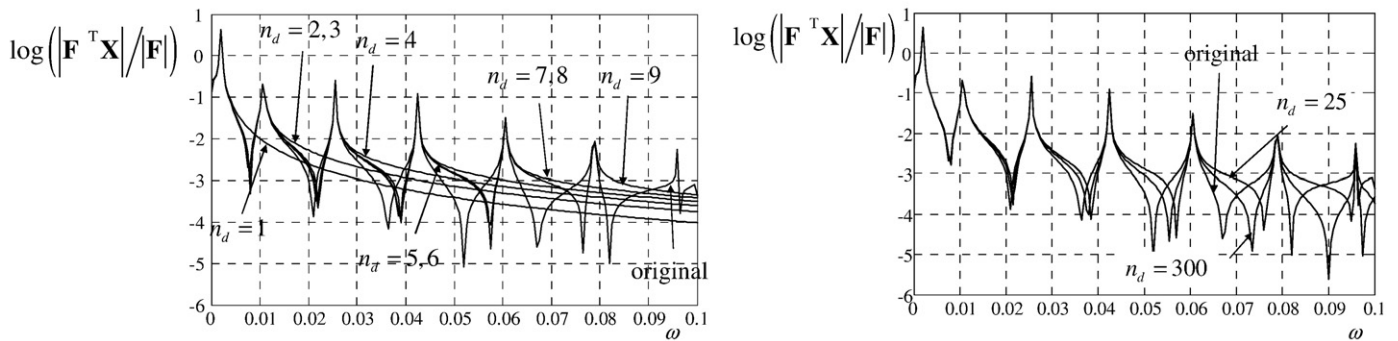


Fig. 3. Approximations using the MS method for load case 1. (Total number of degrees of freedom for the original system and eigenmodes: 4200).

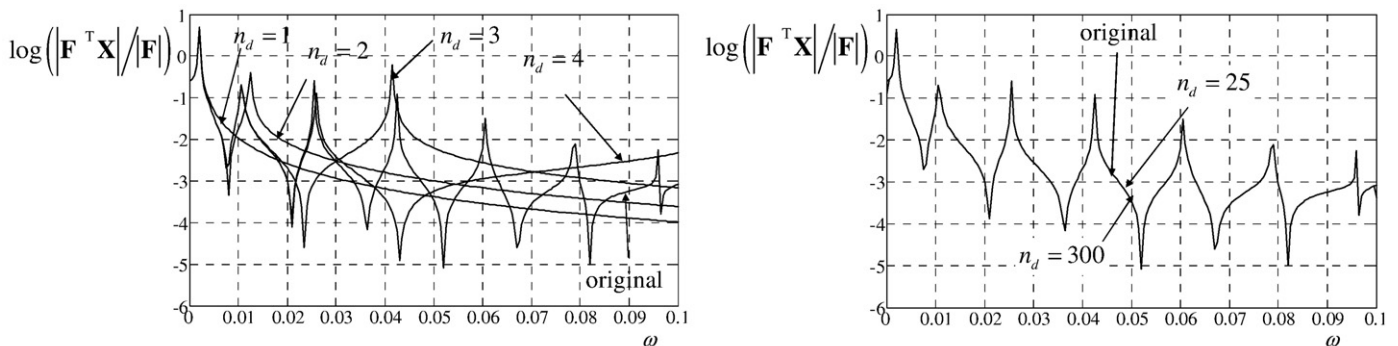


Fig. 4. Approximations using the RV method for loading case 1.

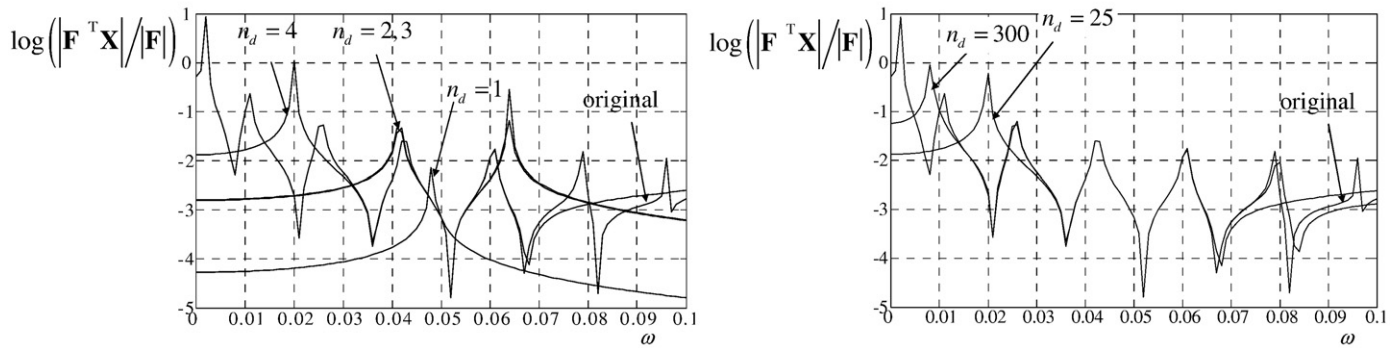


Fig. 5. Approximations using the QSRV method $\omega_c = 0.05$ (rad/s) for case loading 1.

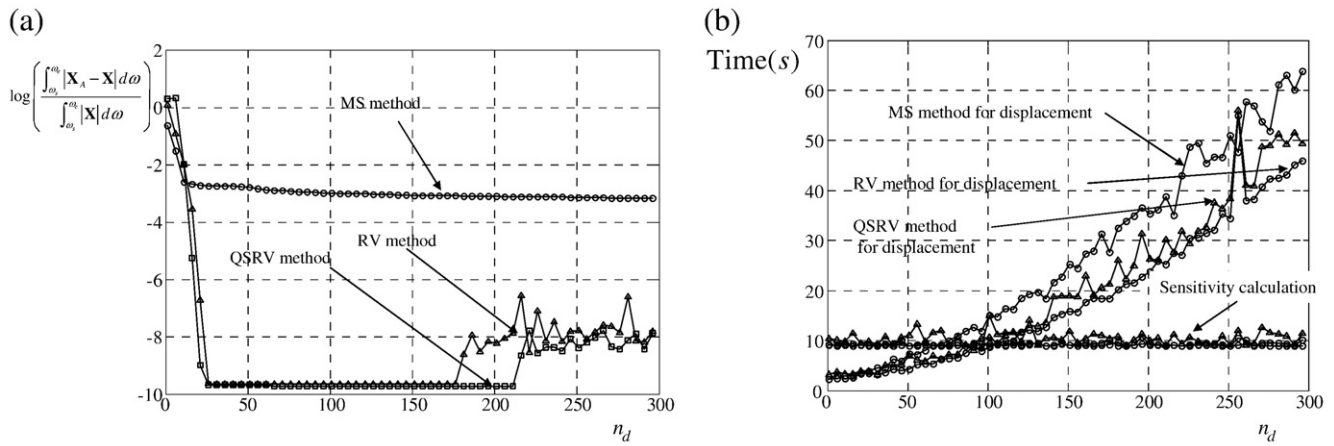


Fig. 6. Comparison of errors and calculation times with respect to the number of used modal reduction bases. (a) Displacement errors and (b) computational times of the three methods. (Displacement calculation time without reduction method (73.326 s) and sensitivity calculation time (9.110 s) with 4200 for the total number of degrees of freedom for the original system).

triangular matrix. The decomposition method is commonly employed in order to save the computation time for the inverse of the stiffness matrix \mathbf{K} in the repeated constructions of the reduction bases. Naturally it also requires more computer memory to save the upper and lower triangular matrices and associated computational time but the computational advantages of the RV method compensate for these additional bundles. As in the MS method, the number of the reduction

bases in the RV method is depending on how accurately we want to approximate the responses of a dynamic structure.

After building the bases of the RV method, the structural response \mathbf{X} is now approximated again.

$$\mathbf{X} \approx \mathbf{X}_A = \Psi \mathbf{Q}. \quad (38)$$

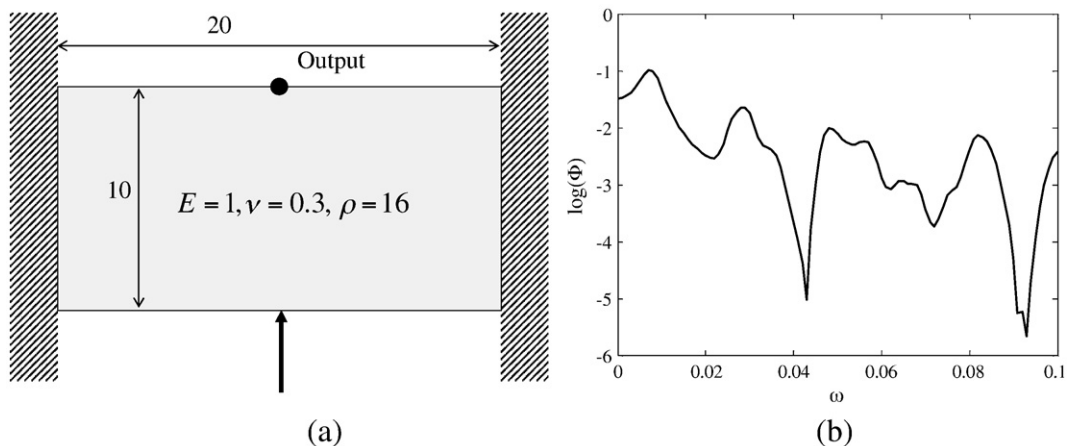


Fig. 7. Forced vibration analysis problem ($\alpha_r = 0.005$, $\beta_r = 0.002$) (The y-direction displacement at the output point is measured.) (a) Problem definition, and (b) FRF of the original system.

Compared with the MS method, the RV method has two distinct points. First, the RV method generates the reduction bases Ψ by considering not only the mass and stiffness matrices of dynamic structures but also the external applied force. Second, the RV method had not yet been applied to topology optimization before this study.

3.4. The quasi-static Ritz vector method (QSRV method: shifted Ritz vector method)

An approach with many similarities to the RV method is so called the quasi-static Ritz vector method approximating better the dynamic response of a dynamic system near at a center frequency of interest

[22,27,29]. In the QSRV method, the Eqs. (35)–(37) of the RV method are modified as follows.

$$\varphi_1 = \frac{1}{\varphi_1^* \mathbf{M} \varphi_1^*} \varphi_1^*, \quad \varphi_1^* \equiv (\mathbf{K} - \omega_c^2 \mathbf{M})^{-1} \mathbf{F} \quad (39)$$

$$\varphi_j^* \equiv (\mathbf{K} - \omega_c^2 \mathbf{M})^{-1} (\mathbf{M} \varphi_{j-1}) \quad (40)$$

$$\text{Orthogonalization : } \varphi_j^{**} \equiv \varphi_j^* - \sum_{k=1}^{j-1} (\varphi_k^{*T} \mathbf{M} \varphi_k^*) \varphi_k^* \quad (41)$$

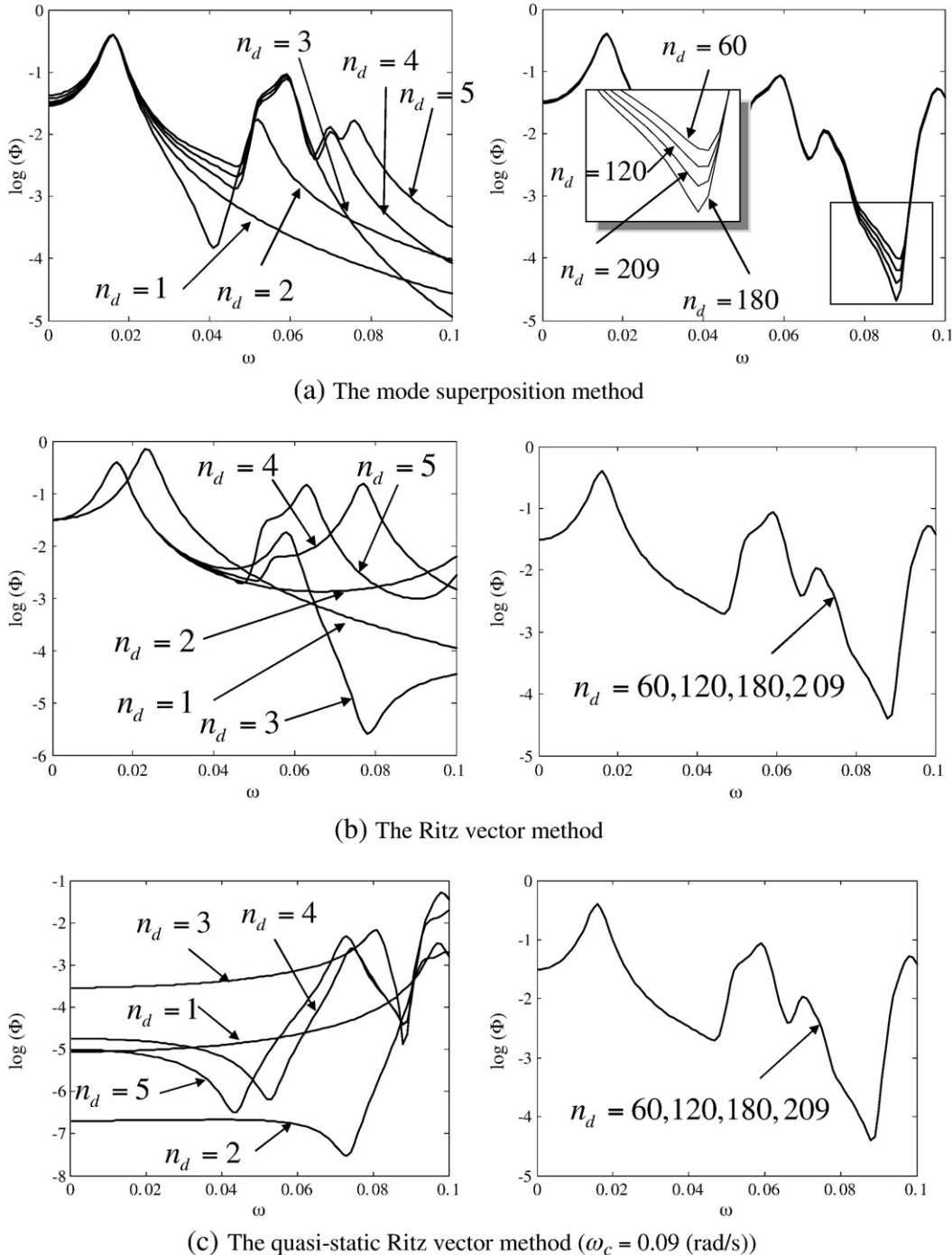


Fig. 8. Comparison of FRFs. (a) The mode superposition method, (b) the Ritz vector method, and (c) the quasi-static Ritz vector method (ω_c = 0.09(rad/s)).

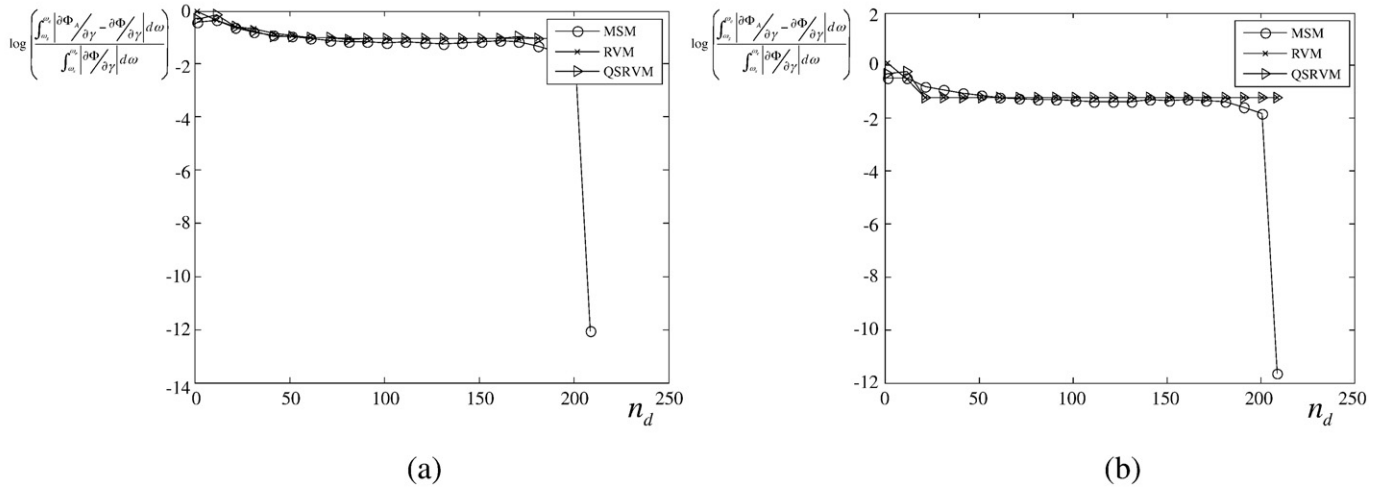


Fig. 9. Comparisons of relative sensitivity value errors with and without the reduction methods. (Frequency domain [0,0.1]) (a) Relative sensitivity value errors with the approximation for the adjoint variable, and (b) relative sensitivity value errors without the approximation for the adjoint variable.

$$\text{Normalization : } \varphi_j = \frac{1}{\varphi_j^{*T} \mathbf{M} \varphi_j^{**}} \varphi_j^{**} \quad (42)$$

where ω_c is the center frequency of interest. The main difference of the method compared with the conventional RV method is that the central frequency, ω_c , is considered in calculating the reduction bases.

If ω_c is set to zero, the QSRV method becomes the RV method exactly. After building the bases of the QSRV method, the structural response \mathbf{X} is approximated again. Other theories of the MS and the RV methods are also applied.

$$\mathbf{X} \approx \mathbf{X}_A = \Psi \mathbf{Q} \quad (43)$$

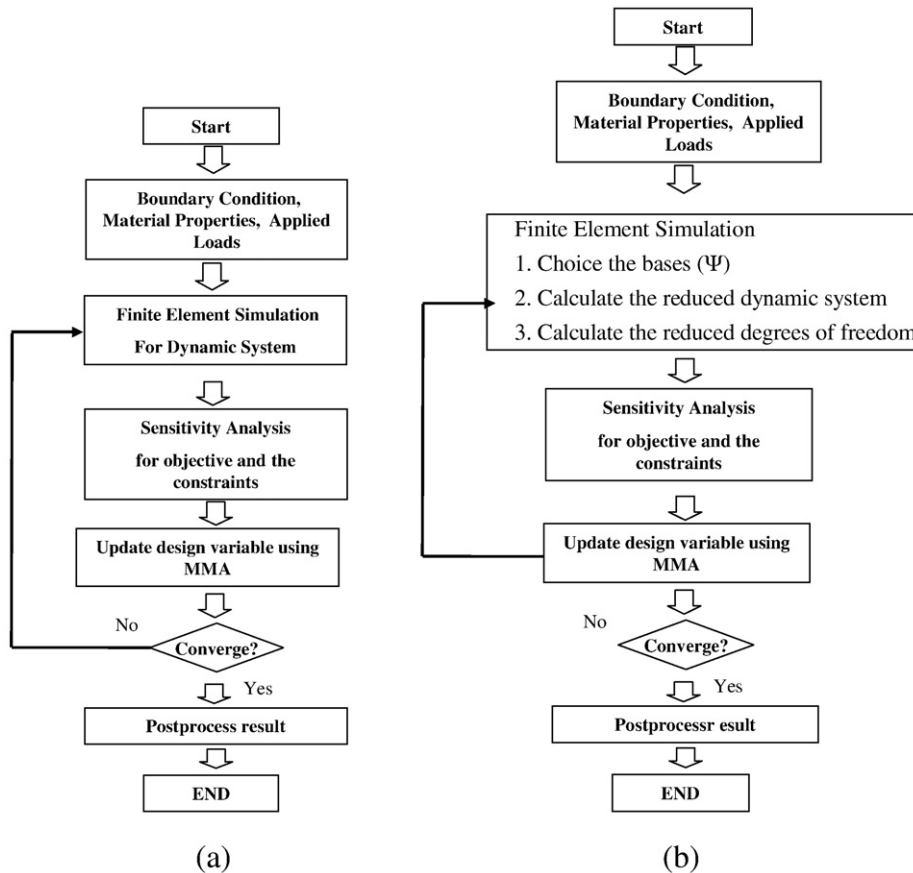


Fig. 10. Present optimization procedures (a) without and (b) with the model reduction scheme.

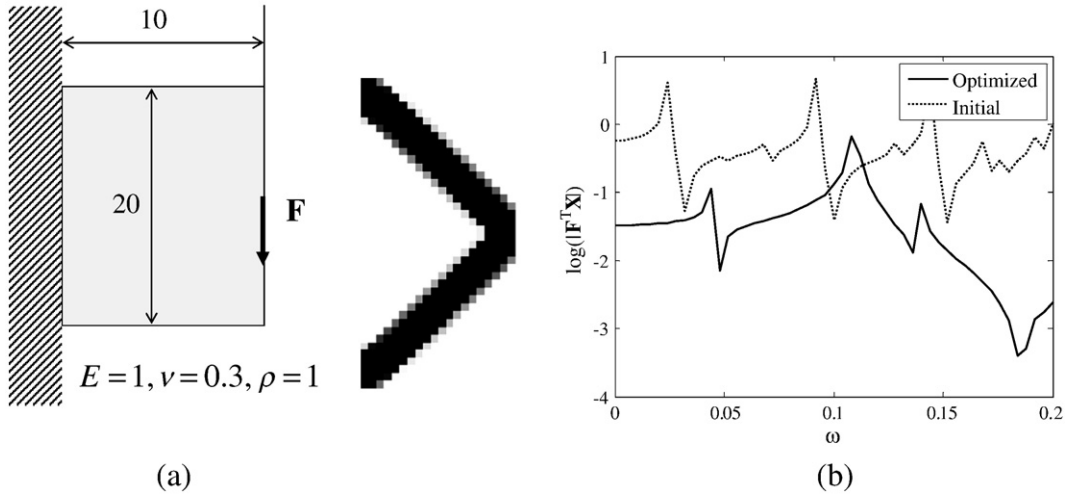


Fig. 11. Benchmark problem without the model reduction scheme. (a) Problem definition ($\omega_s = 0$ (rad/s), $\omega_e = 0.005$ (rad/s), $\Delta\omega = 0.0001$ (rad/s), $\alpha_r = 0.001$, $\beta_r = 0.002$, $F = 1$), (b) an obtained optimization result ($\Phi = 0.0413$ J rad/s, total cpu time: 544 s, iter: 64).

3.5. Comparison of the MR schemes

3.5.1. Analysis example 1: dynamic compliance analysis and sensitivity analyses

To confirm the effectiveness of the MR schemes in structural dynamic analysis, we consider a simple analysis example of a clamped box with two loading cases, as shown in Fig. 1. The geometric size of the analysis domain is 100×20 having 100×20 quad elements. The Young's modulus, Poisson's ratio, and structural density are arbitrarily set to 1 N/m², 0.3 and 1 Kg/m³, respectively.

After solving the reduced dynamic system Eq. (26) for \mathbf{Q} , the structural response \mathbf{X} can be approximated by Eq. (24). The object analysis of Eq. (12) and sensitivity analysis of Eqs. (19) and (20) are further approximated by replacing the exact solution \mathbf{X} with \mathbf{X}_A .

$$\Phi \approx \int_{\omega_s}^{\omega_e} |\mathbf{F}^T \mathbf{X}_A| d\omega \quad (44)$$

$$\frac{d\Phi}{d\gamma_e} \approx \int_{\omega_s}^{\omega_e} 2\text{Real} \left(\lambda_A^T \frac{d\mathbf{S}}{d\gamma_e} \mathbf{X}_A \right) d\omega \quad (45)$$

$$\lambda_A = \frac{-\alpha}{2} \mathbf{X}_A, \alpha = \frac{\mathbf{X}_A^T \mathbf{F}}{|\mathbf{X}_A^T \mathbf{F}|}. \quad (46)$$

To numerically integrate the above first three equations, the numerical integration scheme with equally spaced abscissas is employed.

$$NS = \frac{(\omega_e - \omega_s)}{\Delta\omega} \quad (\Delta\omega : \text{frequency interval}) \quad (47)$$

$$\phi_j = |\mathbf{F}^T \mathbf{X}_A| \quad \text{at } \omega_j = \omega_s + \frac{(\omega_e - \omega_s)}{NS} \times j \quad (48)$$

$$\Phi \approx \frac{\Delta\omega}{2} \phi_1 + \sum_{j=2}^{NS-1} \Delta\omega \phi_j + \frac{\Delta\omega}{2} \phi_{NS} \quad (49)$$

$$\Gamma_j = 2\text{Real} \left(\lambda_A^T \frac{d\mathbf{S}}{d\gamma_e} \mathbf{X}_A \right) \quad \text{at} \quad (50)$$

$$\omega_j = \omega_s + \frac{(\omega_e - \omega_s)}{NS} \times j \quad (51)$$

Fig. 1(b) shows the FRFs of the two loads for the frequency domain $[0, 0.1]$ (rad/s). As expected, there are some peaks due to the resonances of the structure whose eigenfrequencies are calculated in Fig. 2. Some of

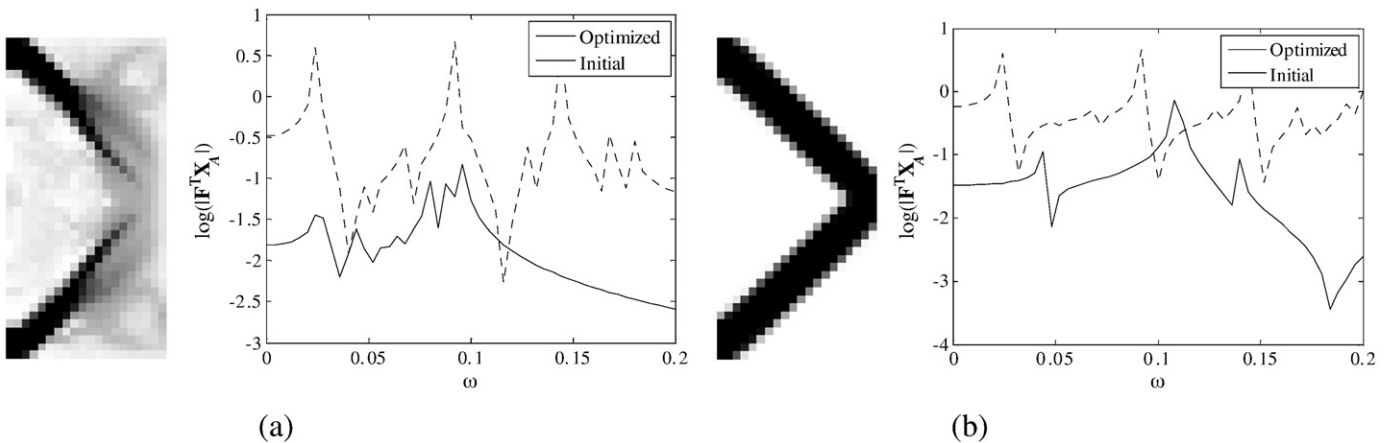


Fig. 12. Optimization results with the MS method. (a) Result with $n_d = 25$ ($\Phi = 0.1101$ J rad/s), (b) a result with $n_d = 1640$ (eigenvalues) ($\Phi = 0.0413$ J rad/s).

the differences among the peaks of the frequency responses shown in Fig. 1(b) of load cases 1 and 2 exist because of the symmetric and antisymmetric eigenmodes shown in Fig. 2. In other words, the load case 1, which excites the nodal points (points at rest at all times) of the symmetric modes, cannot excite the 3rd, 6th, 8th, and 12th symmetric modes. To understand the numerical efficiencies and characteristics of the three MR schemes, the FRFs of Fig. 1(b) are now approximated with each method shown in Figs. 3–5, and the computation times for the approximated frequency responses and approximated sensitivity values are compared in Fig. 6. Here due to the truncation error and the round-off error, the inclusion of more than 160 bases in the RV method and the QSRV method does not guarantee the improvements of accuracy in Fig. 6 (a). As shown in Fig. 3 the FRF for the load case 1 is approximated using the MS method. Because the reduction bases used for the MS method are eigenmodes of the original system (Fig. 1), it can be postulated that the accuracy of the approximated FRF has been improved with respect to the number of employed eigenmodes as shown in Fig. 3. An interesting fact found in this specific example is that the usage of the 3rd, 6th, 8th modes (shown in Fig. 2) does not improve the accuracy of the FRF for load case 1 when exciting the nodal points of the symmetric modes. From these analyses, we found that if an external loading is applied near the nodal points of the eigenmodes, the inclusion of the corresponding eigenmodes slightly improves the accuracies of the approximated FRFs. Numerically, with the MS method it is observed that the low eigenmodes should be used even if a higher frequency domain is the only domain of interest as shown in Fig. 2. In other words, even if the FRFs at only higher frequency domain are required, the MS method requires the lower eigenmodes to approximate the FRF, as shown in Fig. 3(b).

In Fig. 4, the FRF of Fig. 1(b) is approximated using the RV method. Similar to the MS method, the accuracy of the RV method is improved with respect to the number of employed Ritz vectors. However, the approximation of the RV method is quite different than that of the MS method in this specific example. The reduction bases of the RV method generated by considering the external force, mass, and stiffness matrices of the original system are not the eigenmodes. Therefore, the number of approximated resonance peaks of the system is not in proportion to the number of the Ritz vectors, as shown in Fig. 4. Furthermore, it seems that in this specific example, the approximation accuracies of $n_d=25$ and $n_d=300$ for the RV method, which are arbitrary chosen numbers, are better than those of the MS method.

As a variation of the RV method, the QSRV method is also tested to approximate the FRF of Fig. 1(b) with $\omega_c=0.05$ (rad/s). Because it generates the reduction bases considering the dynamic stiffness with the center frequency ω_c , it approximates the original FRF at the specific center frequency more effectively than the MS or the RV methods do, as shown in Fig. 5.

Fig. 6 shows comparisons of the computation times and errors of the three MR schemes. As expected, the accuracies of the schemes are improved with respect to the number of employed reduction bases. Because the MS method requires times to calculate the eigenvalues, it takes more time than the RV and QSRV methods. Because the sensitivity analysis Eq. (23) is the same, the calculation times for the sensitivity analyses do not change. It can be also noted that it takes more time than the analysis without the reduction methods with too many reduction bases.

3.5.2. Analysis example 2: analysis of force vibration response (non-self adjoint system)

Next, we extend our studies of the underlying reduction theories into the non-self adjoint system. In the first numerical example, we considered the dynamic compliance which is a self-adjoint problem with the adjoint variables in proportion to the structural responses. If the structural responses of some points excluding the excitation points are considered, the adjoint variables are no longer proportional to the structural responses (non-self adjoint) and should be calculated by the Eq. (22) for the sensitivity analysis of the Eq. (45). Thus, for

the MR schemes, the following approximated solutions should be used.

$$\Phi \approx \int_{\omega_s}^{\omega_e} \mathbf{X}_A^T \mathbf{L} \bar{\mathbf{X}}_A d\omega \quad (52)$$

$$\text{Approach 1: } \lambda_A = -\underbrace{\Psi^T (\Psi^T \mathbf{S} \Psi)^{-1} (\Psi^T \mathbf{L} \bar{\mathbf{X}}_A)}_{\text{The reduced dynamic stiffness matrix}} \quad (53)$$

$$\text{Approach 2: } \lambda_A = -\mathbf{S}^{-1} \mathbf{L} \bar{\mathbf{X}}_A \quad (54)$$

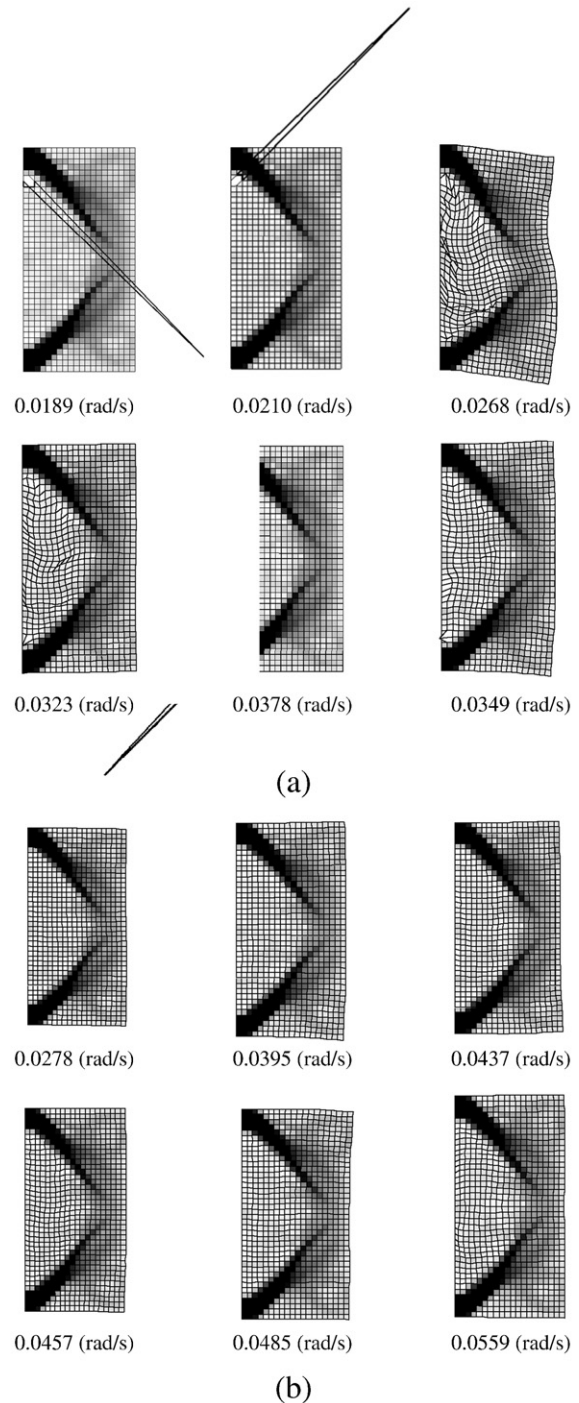


Fig. 13. (a) First 6 eigenmodes for the result shown in Fig. 12(a); they are locally vibrating modes, (b) First 6 eigenmodes of (a) with the modified material interpolation proposed in [9]; $E(\gamma) = E_0\gamma^n$ for $\gamma \geq 0.1$ or $E_0\gamma/100$ for $\gamma < 0.1$.

$$\frac{d\Phi}{d\gamma_e} \approx \int_{\omega_s}^{\omega_e} 2\text{Real}(\lambda_A^T \frac{d\mathbf{S}}{d\gamma_e} \mathbf{X}_A) d\omega \quad (55)$$

where \mathbf{L} is a $n \times n$ matrix returning the displacement of the output point by multiplying the displacement vector. Note that with the Eq. (53) the adjoint variable λ is approximated as λ_A with both the approximated solution \mathbf{X}_A and the approximated dynamic stiffness matrix; consequently the calculated λ_A may be adversely modified. Furthermore, we found that using Eq. (54) without any approximation to the dynamic stiffness matrix is possible, but it requires \mathbf{S}^{-1} for a considered frequency domain, which produces the heavy computation time and what we want to avoid by using the MR schemes. To see the effect of these two approximations for the adjoint variable, the forced vibration analysis shown in Fig. 7 is considered, whose objective value is used to measure the absolute value of the displacement at the output point. Figs. 7(b) and 8 plot the FRFs without and with the MR schemes, respectively. Fig. 9 shows the errors of the sensitivity values with and without the approximation for the adjoint variable. As expected, the approximation of the adjoint variable using the Eq. (53) induced some approximation errors in the sensitivity value. Therefore, it is expected that its application to topology optimization may produce a slow convergence, especially for a higher excitation.

4. Topology optimization examples

To show and compare the effectiveness of the MR schemes, this section provides several numerical examples. The optimization procedures in Fig. 10 are implemented in the framework of MATLAB and the design domains and material properties are arbitrarily chosen

to show the potential of the MR schemes in topology optimization. For the convergence criteria, the following absolute change of design variables of two sequential optimization iterations are considered and the maximum optimization iteration is set to 600.

$$\max (|\gamma_{iter} - \gamma_{iter-1}|) < 0.001 \text{ and the maximum iteration} = 600 \quad (56)$$

where the iteration number is denoted by iter.

4.1. Example 1: two bar example

For the first optimization example, the topology optimization of minimizing the dynamic compliance of a plane structure with unit thickness as shown in Fig. 11(a) is considered. The design domain is a 10×20 rectangular box with 20×40 quad elements inside. The left boundary is clamped and a point load ($F = 1$ N) is applied to a node in the middle of the right boundary. The number of total independent modal generalized displacements and total number of free degrees of freedom is 1640. The Young's modulus, Poisson's ratio, and structural density of the solid are set to 1 N/m², 0.3, and 1 kg/m³, respectively. The optimization formulation is then defined as follows.

$$\text{Min } \Phi = \int_{\omega_s}^{\omega_e} |\mathbf{F}^T \mathbf{X}| d\omega \quad (57)$$

$$\text{S.t. } \sum_{e=1}^N \gamma_e v_e \leq V^*$$

where the design variable and volume of the e -th element are γ_e and v_e , respectively. The total number of elements is $N = 800$. The volume

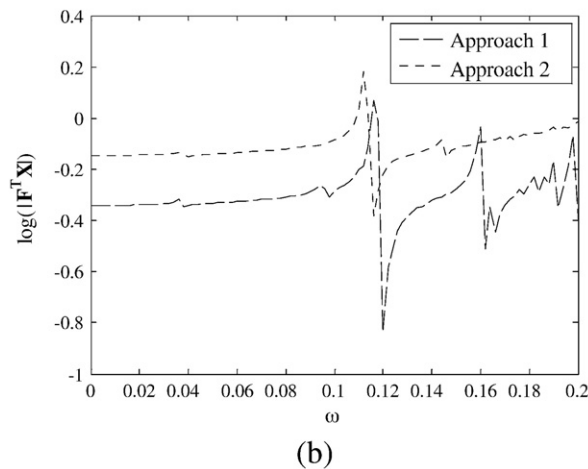
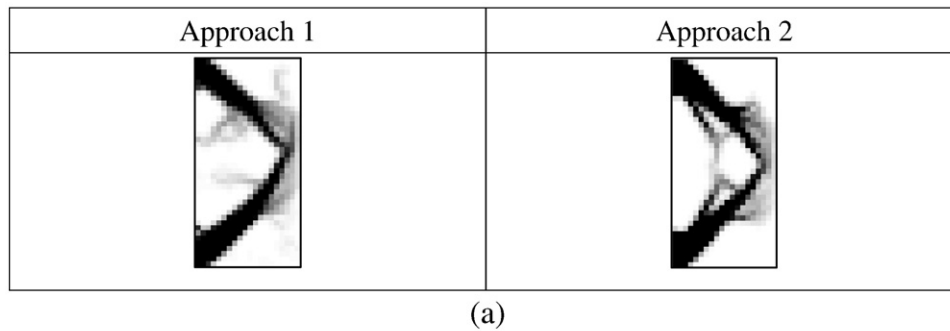


Fig. 14. Optimization results with the interpolation function of Fig. 13(b) removing the localized modes. (a) Optimization results (Approach 1: the interpolation function eliminating the localized modes both to the dynamic compliance minimization problem and to the eigenfrequency calculation and Approach 2: the interpolation function eliminating the localized modes only to the eigenfrequency calculation) and (b) frequency response curves.

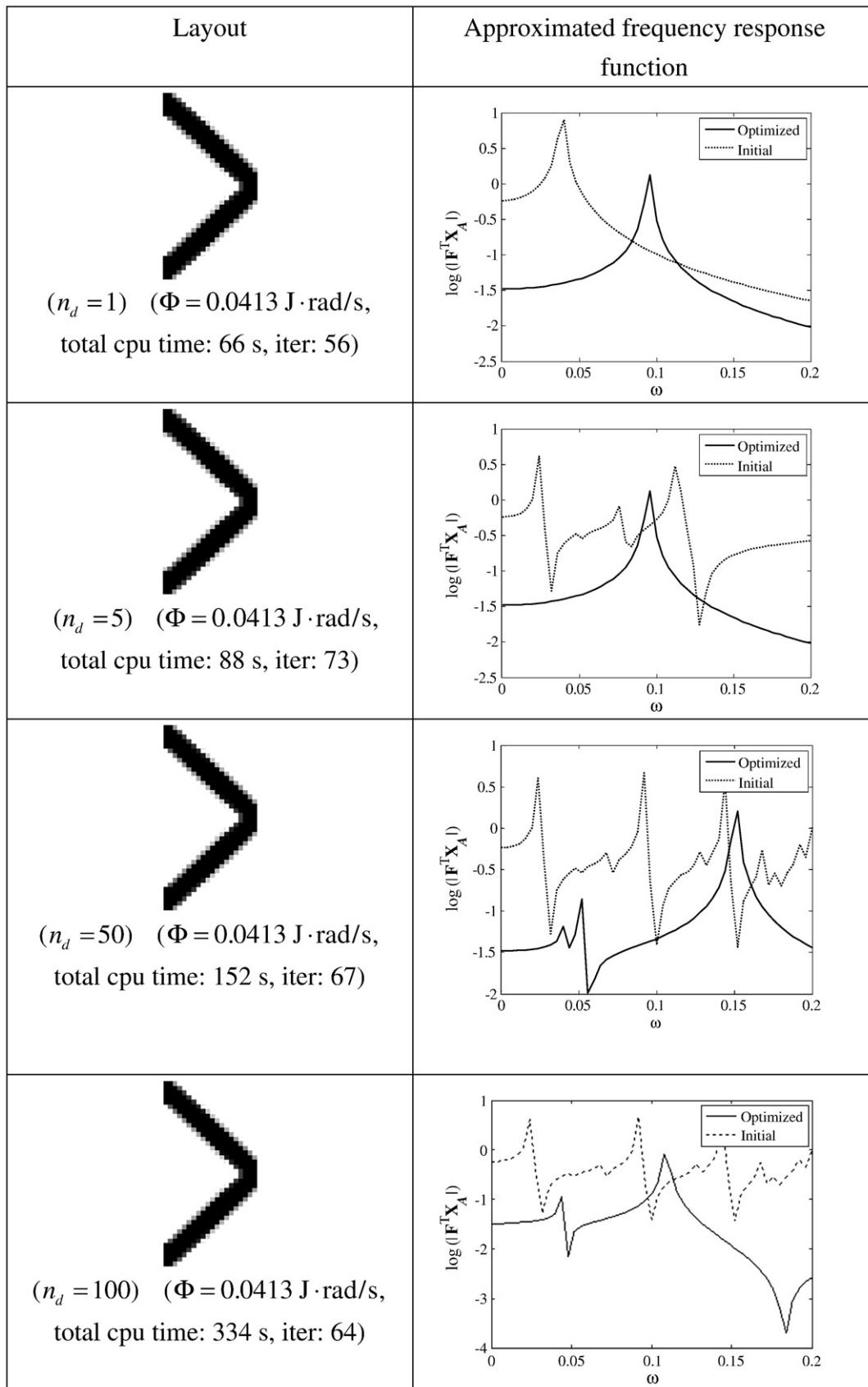


Fig. 15. Optimization results with the RV method.

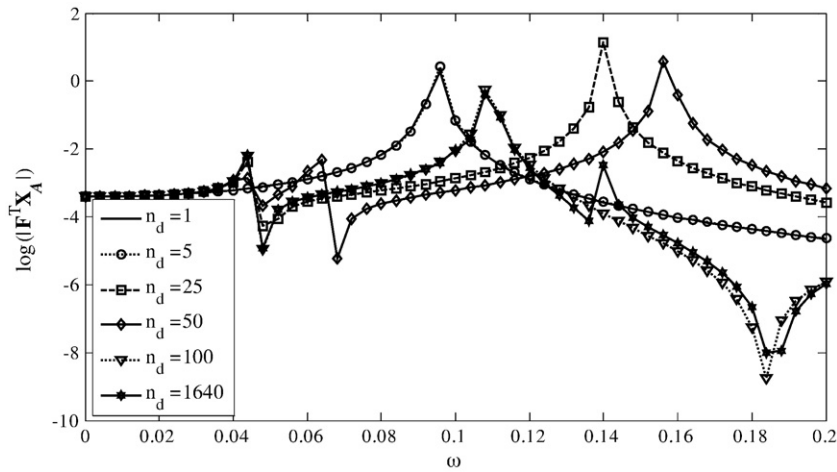


Fig. 16. Approximated frequency response functions for $n_d = 1$ with many Ritz bases.

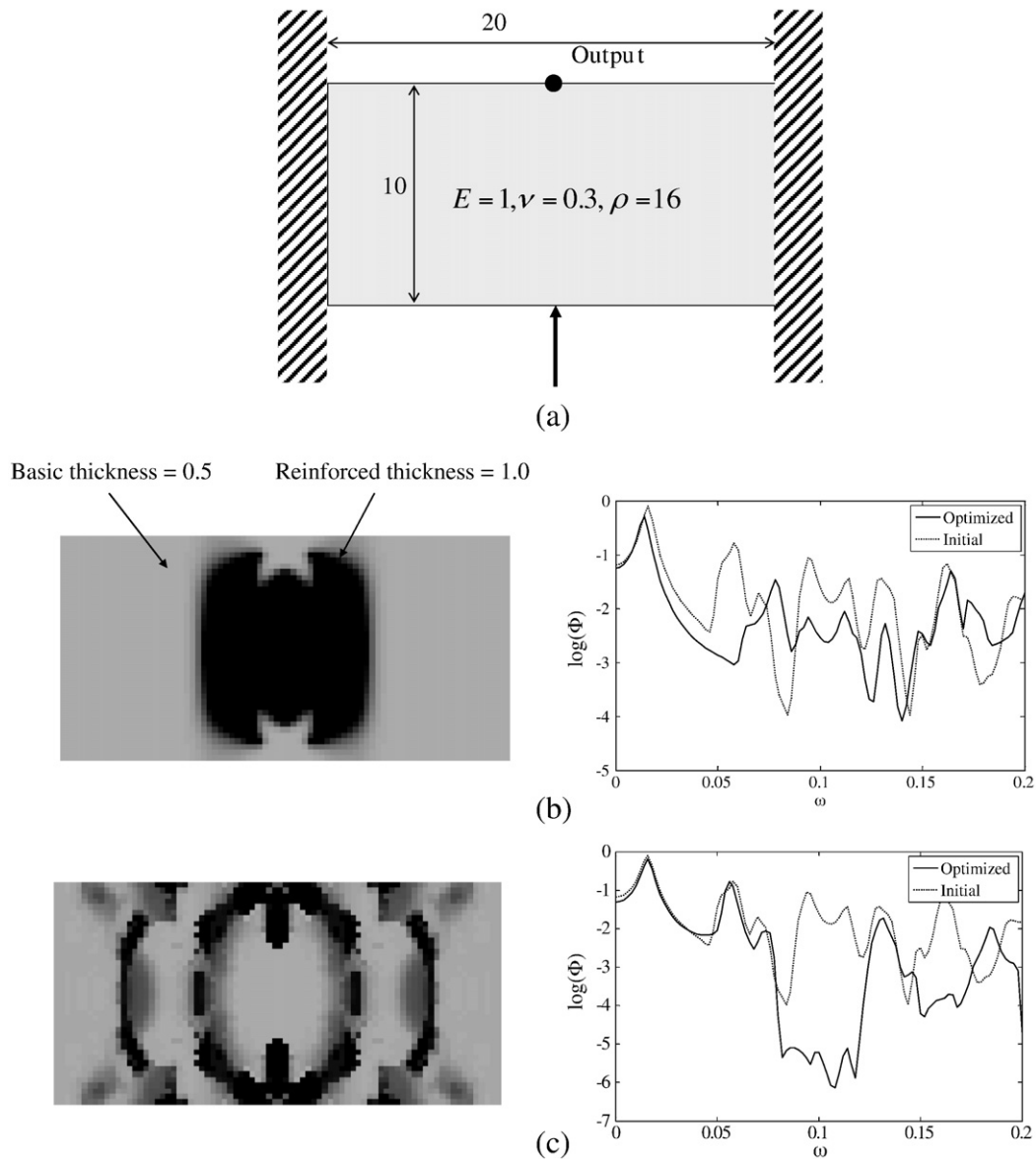


Fig. 17. Reinforcement design example with forced vibration. (a) Geometry definition (basic thickness = 0.5, $\alpha_s = 0.005$, $\beta_s = 0.002$) and (b) an optimization result for the first frequency interval ($\omega_s = 0.02$, $\omega_e = 0.04$, $\Delta\omega = 0.0004$, $\Phi = 0.1243$ (m rad/s), iteration = 103, total cpu time = 2707 s, time per iteration = 26.2 s), and (c) an optimization result for the second frequency interval ($\omega_s = 0.08$, $\omega_e = 0.12$, $\Delta\omega = 0.0008$, $\Phi = 1.047 \times 10^{-4}$ (m rad/s), iteration = 536, total cpu time = 14,509 s, time per iteration = 27.06 s).

limit V^* is constrained to be less than 30% of the design domain. First, the dynamic compliance for the low range $[0, 0.005]$ (rad/s), which is located at the left side of the first frequency resonance of the initial design having 0.3 for γ_e , is minimized without any MR scheme in Fig. 11(b). As shown in Fig. 11(b), the optimal structure is similar to the design minimizing the static compliance, because minimizing the dynamic response of the considered frequency domain stiffens the structure. In Fig. 12, the optimization problem is solved by employing the MS method. Because the considered frequency interval is placed left of the first resonance frequency, the first 25th eigenmodes are sufficient from an engineering point of view and selected as the bases of the MS method, as shown in Fig. 12(a). Comparing the dotted lines of the initial FRFs in Figs. 11(b) and 12(a,b), it is found that the first 25 eigenmodes represent the frequency response of the initial design quite accurately. However, after 600 iterations, we obtain the structure of Fig. 12(a) which has a lot of gray elements. Although the upper and lower parts appear near the clamped boundary, details for the right side do not appear. Furthermore, the structural response of the optimized design shown in Fig. 12(a) is unsatisfactory, which implies that the first 25 eigenmodes are not sufficient. To investigate

this result further and the peculiar FRFs, the first 6 eigenmodes of the layout of Fig. 12(a) are calculated and investigated in Fig. 13. Here, these calculated eigenmodes are shown to be locally vibrating modes due to the rapid decreasing of the stiffness to the mass ratios around void regions; these local vibrating modes were recently found in the SIMP approach [9,17,25]. From these numerical observations, these highly localized vibrating eigenmodes can be concluded to inevitably appear in the SIMP approach, and they halt optimization processes with the MS method. There are some interpolation functions eliminating these modes [9]. By modifying the interpolation functions of stiffness matrix or mass matrix, it is known that these localized vibrating modes can be suppressed. Therefore one of the interpolation functions in [9] is tested in Fig. 13(b) and Fig. 14. Although it is definitely eliminating these localized vibrating modes, owing to the lack of bases (higher mode truncation), it is still hard to find out some details in designs and Fig. 14. Furthermore, when the mode switching phenomena among calculated eigenmodes in the MS method or the order switching of eigenvalues occur during an optimization process, the approximation accuracy of the FRFs with the MS method is also affected. However, if all the eigen modes, which mathematically

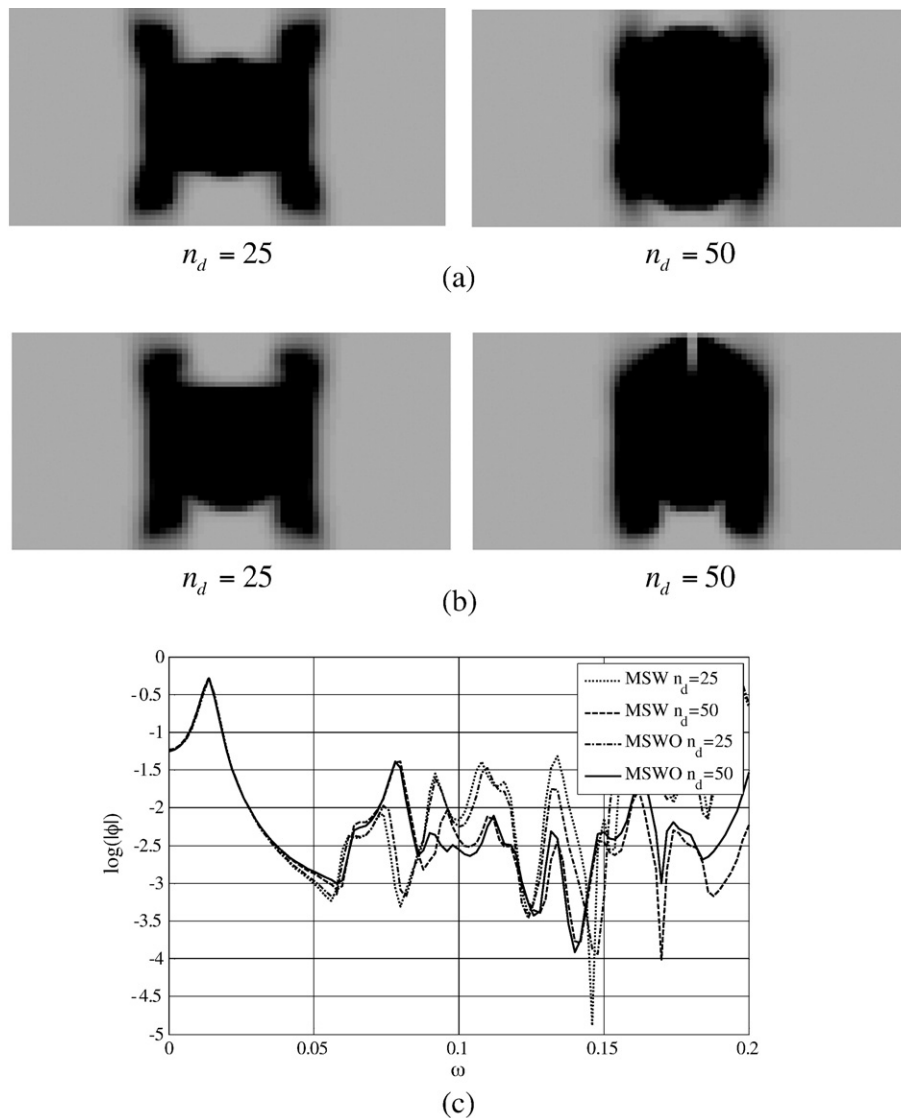


Fig. 18. Results with the mode superposition method for the first frequency domain. (a) Results with the adjoint variable approximation using Eq. (53), (b) results without the adjoint variable approximation using Eq. (54) and (c) frequency response functions. (MSW: the MS method with the adjoint variable approximation using Eq. (53) and MSWO: the MS method without the adjoint variable approximation using Eq. (54)).

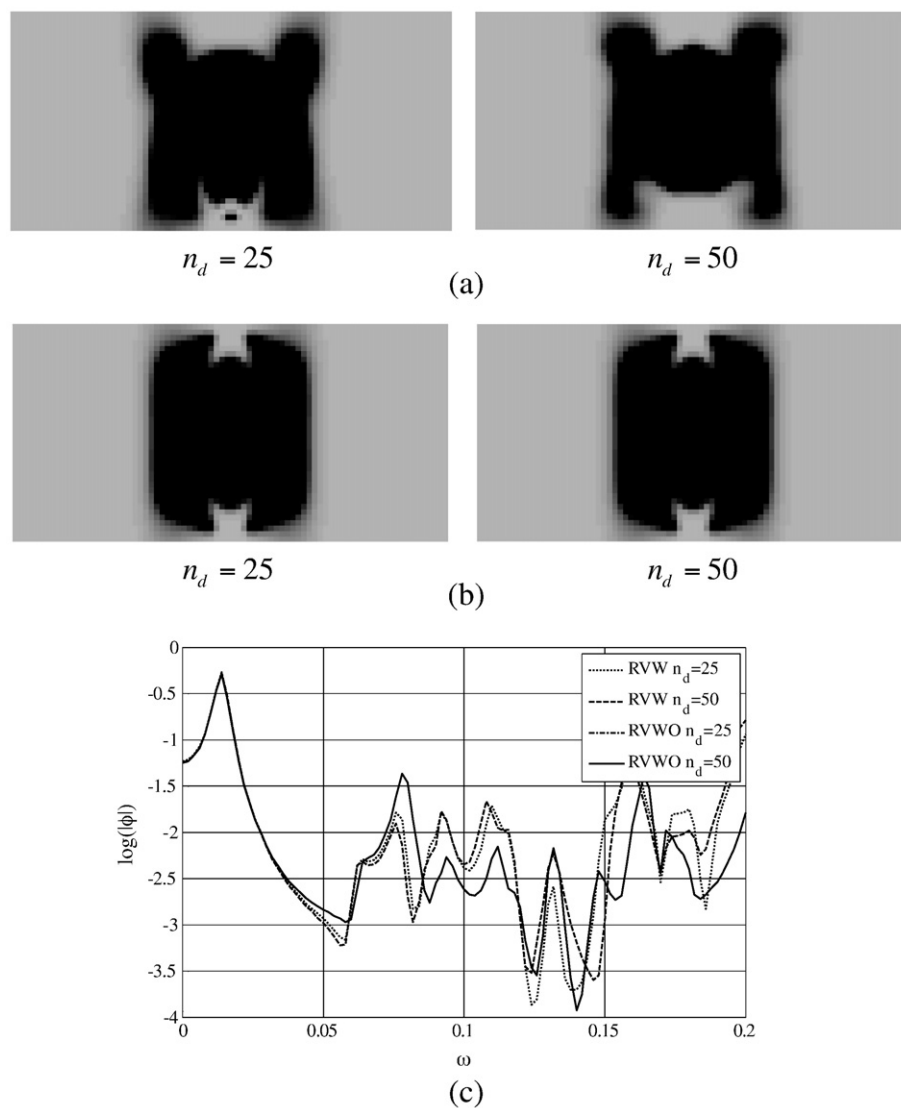


Fig. 19. Results with the Ritz vector method for the first frequency domain. (a) Results with the adjoint variable approximation using equation (53), (b) results without the adjoint variable approximation using equation (54) and (c) the frequency response functions. (RVW: the RV method with the adjoint variable approximation using equation (53) and RVWO: the RV method without the adjoint variable approximation using equation (54). The curves of RVWO $n_d=25$ and $n_d=50$ are almost identical.)

Table 1
Optimization results for the first frequency range with the adjoint variable approximation with Eq. (53).

Method		Iteration	Objective function value (m rad/s) ^a	Total cpu time (s)	Time per iter (s)
Standard method		103	0.1243	2707	26.2
MS method	$n_d = 25$	76	0.1227 (0.1268)	207	2.7
	$n_d = 50$	81	0.1175 (0.1271)	759	9.3
RV method	$n_d = 25$	76	0.1322 (0.1260)	212	2.7
	$n_d = 50$	141	0.1315 (0.1253)	634	4.4

^a The objective value in parenthesis is the objective values recalculated without model reduction.

Table 2
Optimization results for the first frequency range without the adjoint variable approximation with Eq. (54).

Method		Iteration	Objective function value (m rad/s) ^a	Total cpu time (s)	Time per iter (s)
Standard method		103	0.1243	2707	26.2
MS method	$n_d = 25$	81	0.1175 (0.1261)	759	9.3
	$n_d = 50$	176	0.1281 (0.1254)	1777	10.0
RV method	$n_d = 25$	138	0.1304 (0.1244)	1470	10.6
	$n_d = 50$	138	0.1304 (0.1244)	1463	10.3

^a The objective value in parenthesis is the objective values recalculated without model reduction.

means using the full rank bases, are considered, it is possible to get the exact same result of Fig. 11(b) despite the problem of localized eigenmodes issue as shown in Fig. 12(b); however, with all the eigenmodes, the MS method is not more efficient than a method without an MR scheme.

We shall now examine the features of the RV method by testing the problem of Fig. 11 with many Ritz bases. As previously explained, the RV method generates its reduction bases by considering static displacements, which prevents the localized eigenmode bases observed in the MS method. Thus, very stable convergences are obtained in Fig. 15, although negligible differences in the layouts are observed. It is even possible to use $n_d = 1$, where the size of the dynamic stiffness matrix is 1. The total computation time for the optimization procedure with $n_d = 1$ is reduced almost to one-tenth compared with the computation time of the result in Fig. 11. To test these optimized results further, the result with $n_d = 1$ is reanalyzed by increasing the number of bases in Fig. 16, and the FRF of the layout is found to almost identical to the result without the MR scheme as shown in Fig. 11(a). If a higher frequency domain is of interest, it is essential to use a sufficient number of bases for the RV method or to employ the QSRV method representing FRF near a center frequency.

4.2. Example 2: wave transmit structure example

For the second optimization example, a wave transmit structure example (non-self adjoint example) with a 20×10 design domain (Fig. 17) is considered. For the boundary conditions, the left and right boundaries of the design domain are clamped, and the upper direction point load is applied to a node in the middle of the bottom line. The reinforcement material with unit thickness is distributed to minimize the y-direction displacement at the output point (Fig. 17). Unlike the previous example, the design variables denote the reinforcement thicknesses of the design domain with a basic thickness. In other words, the basic structure with 0.5 thickness is reinforced by an additional layer with a thickness of 1. The optimization formulation is set as follows.

$$\text{Min } \Phi = \int_{\omega_s}^{\omega_e} |\mathbf{X}_{\text{output}}| d\omega \quad (58)$$

$$\text{S.t. } \sum_{e=1}^N \gamma_e v_e \leq V^*$$

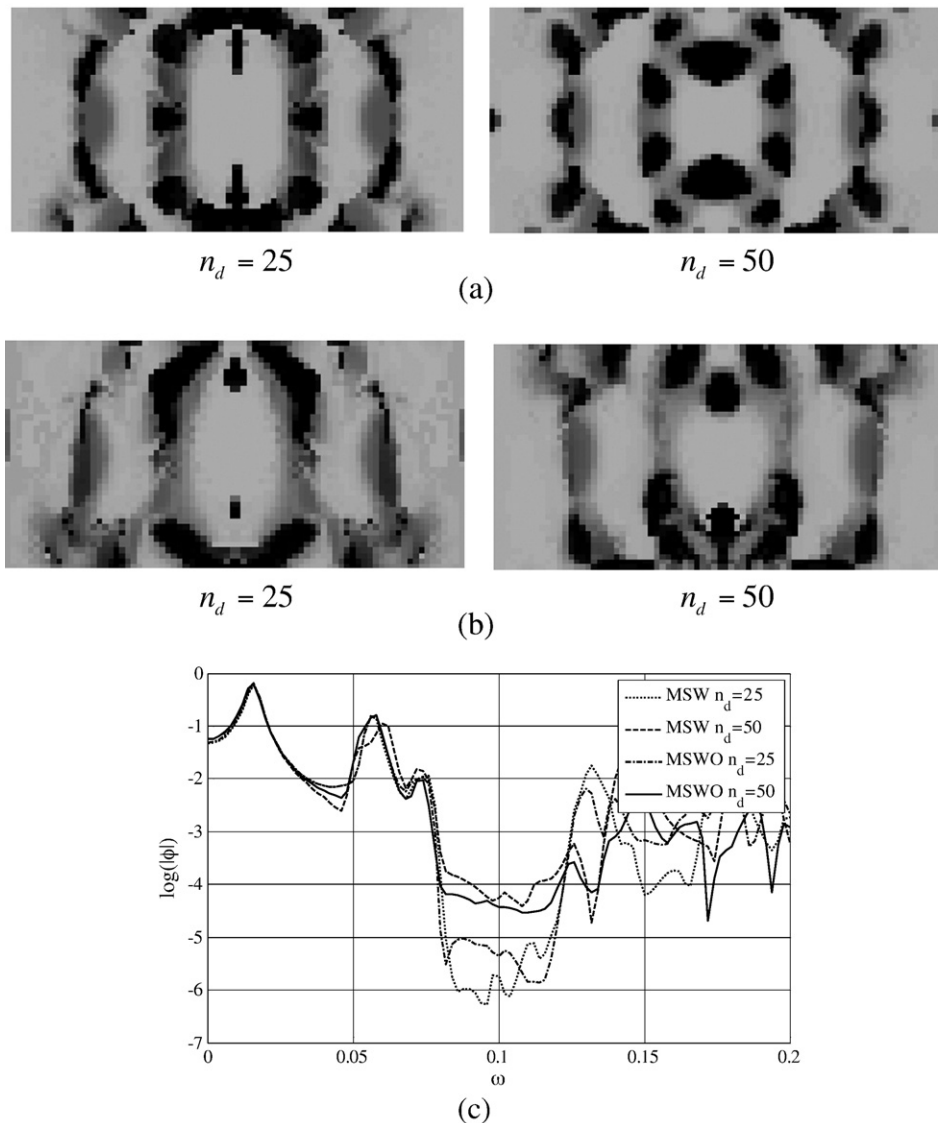


Fig. 20. Results with the mode superposition method for the second frequency domain. (a) Results with the adjoint variable approximation using Eq. (53), (b) results without the adjoint variable approximation using Eq. (54) and (c) the frequency response functions. (MSW: the MS method with the adjoint variable approximation using Eq. (53) and MSWO: the MS method without the adjoint variable approximation using Eq. (54)).

where γ_e represents the e -th reinforcement thickness varying from 0 to 1. Fig. 17 shows the FRFs of the initial design and the optimal layout from the density based approach with no MR scheme for the two frequency domains [0.02, 0.04] and [0.08, 0.12]. Obtaining the layout design for the first frequency domain, took almost 2700 s and 103 optimization iterations. The optimized objective value is $\Phi = 0.1243$ (m rad/s). For the second frequency interval, the optimal design of $\Phi = 1.047 \times 10^{-4}$ (m rad/s) is obtained after 536 iterations, which takes 14,509 s. As illustrated here, the responses are optimized for the two given frequency intervals.

Using the MS and RV methods, the optimization problems for the first frequency domain, i.e., [0.02, 0.04], is solved as shown in Figs. 18 and 19; the detailed information is listed in Tables 1 and 2. The QSRV method is not attempted here because the considered frequency domain is a relatively low frequency range. In this particular reinforcement design problem, as the highly localized mode issue observed in Void areas does not appear, the MS method can also be applied. As shown here, using the two MR schemes, several local optima are obtained. It is of interest that the presented designs using the MR schemes are inferior to the designs without the MR schemes

for the first low frequency domain. This is because 1) the frequency response curves are sufficiently smooth and 2) the exact FRFs cannot be presented by the MR schemes. Furthermore, as stated before, there are two optimization strategies for this problem depending on the adjoint variable formulation; first, the optimization can be performed using the Eq. (53), and second, it is possible to use the adjoint variable with the Eq. (54) without any reduction to the dynamic stiffness matrix. From the computational point of view listed in Tables 1 and 2, the former is definitely a fast way to use Eq. (53). However, our results show that approximating the sensitivity value can affect the number of optimization iterations and optimized layouts. Figs. 18 and 19, Tables 1 and 2 compare the optimization results for the two model reduction bases ($n_d = 25$ and $n_d = 50$) with the two formulations of Eqs. (53) and (54). Using the Eq. (54) definitely took more time because it requires the direct inversions of the dynamic stiffness matrix \mathbf{S} . However, in this particular example, using Eq. (53) is prone to obtaining local optima using the Eq. (53). For the second frequency domain, i.e., [0.08, 0.12], similar observations to the results for the first frequency domain can be made, except that the QSRV and the RV methods provide better solutions in terms of the objective function as

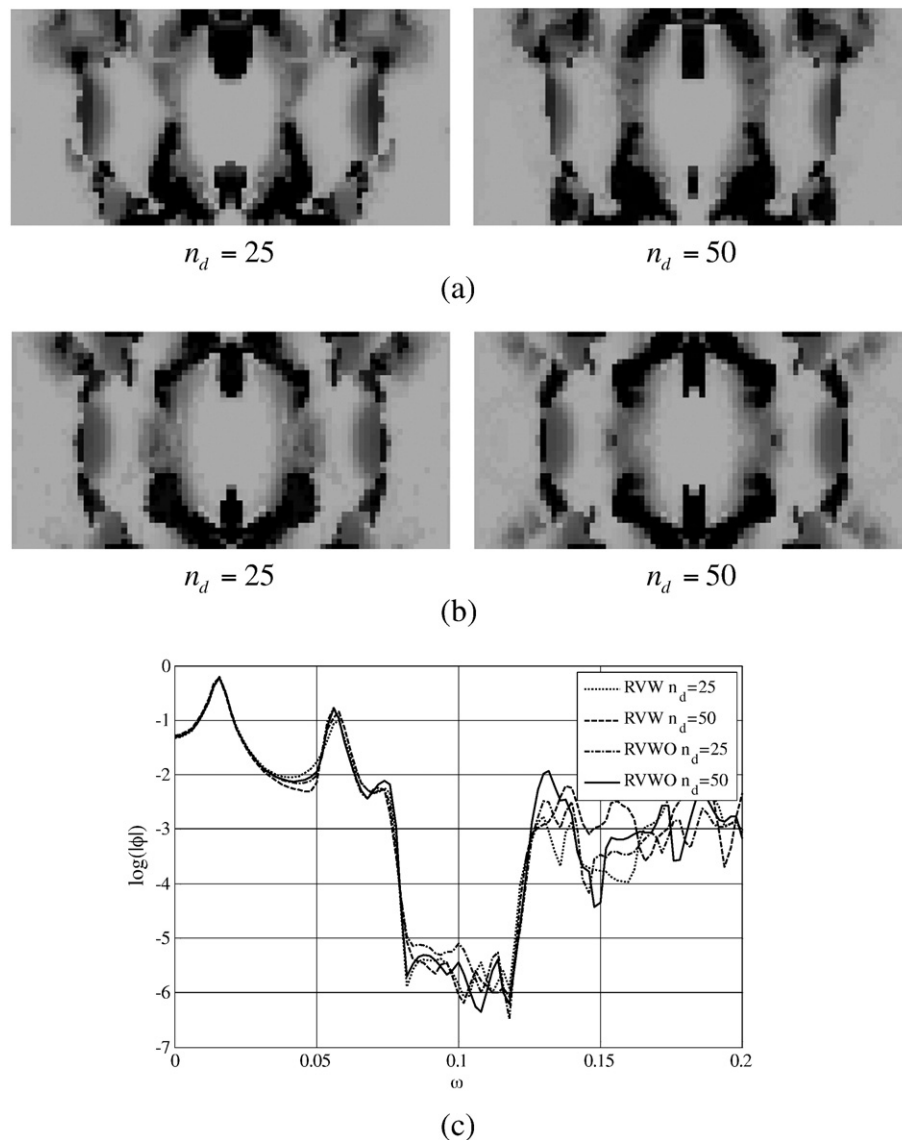


Fig. 21. Results with the Ritz vector method for the second frequency domain. (a) Results with the adjoint variable approximation using Eq. (53), (b) results without the adjoint variable approximation using Eq. (54) and (c) the frequency response functions. (RVW: the RV method with the adjoint variable approximation using Eq. (53) and RVWO: the RV method without the adjoint variable approximation using Eq. (54)).

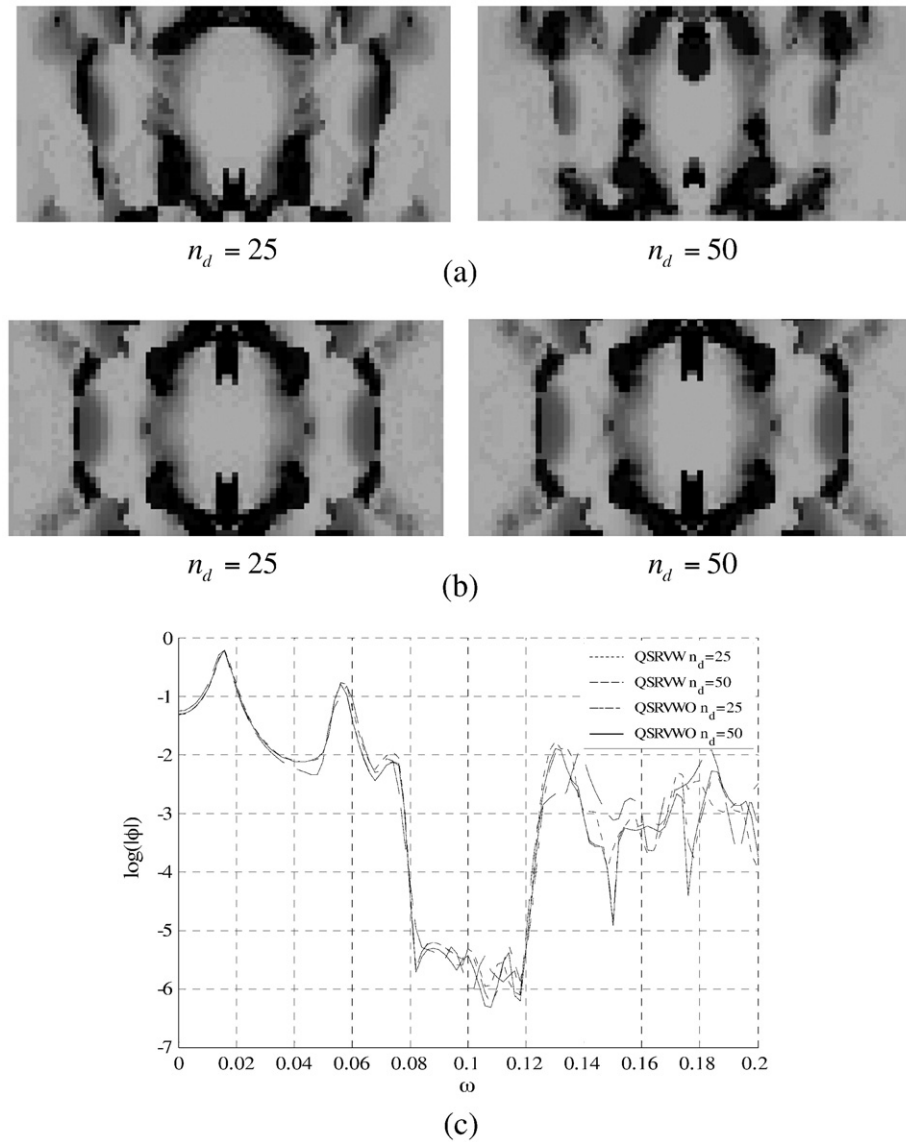


Fig. 22. Results with the quasi-static Ritz vector method for the second frequency domain. (a) Results with the adjoint variable approximation using Eq. (53), (b) results without the adjoint variable approximation using Eq. (54) and (c) the frequency response functions. (QSRVW: the QSRV method with the adjoint variable approximation using Eq. (53) and QSRVWO: the QSRV method without the adjoint variable approximation using Eq. (54)).

shown in Figs. 20–22, Tables 3 and 4. Because the shapes of the FRFs for the second frequency domain are intricate and noisy, it is likely that approximating the responses removes or filters the oscillations of the FRFs in the second frequency domain and helps the optimizer to find another local optima. Furthermore, some gray elements are

observed especially for the second frequency domain. To remove these gray elements, this paper tests the effect of the inclusion of a penalty, $\sum \gamma(1 - \gamma)$, to the objective function in Fig. 23. As expected, although we can remove these gray elements, the designs in Fig. 23 are not good as the designs with gray elements. In conclusion, the

Table 3

Optimization results for the second frequency range with the adjoint variable approximation with Eq. (53).

Method		Iteration	Objective function value (m rad/s) ^a	Total cpu time (s)	Time per iter (s)
Standard method		536	1.047×10^{-4}	14,509	27.0
MS method	$n_d = 25$	600	1.3740×10^{-4} (1.2108×10^{-4})	1673	2.7
	$n_d = 50$	600	3.7492×10^{-4} (20.0000×10^{-4})	759	9.3
RV method	$n_d = 25$	260	6.3444×10^{-5} (5.6229×10^{-5})	1003	3.8
	$n_d = 50$	600	7.2362×10^{-5} (6.5527×10^{-5})	3835	6.3
QSRV method	$n_d = 25$	600	7.4960×10^{-5} (7.3358×10^{-5})	2505	3.4
	$n_d = 50$	600	9.7689×10^{-5} (8.4243×10^{-5})	4325	7.2

^a The objective value in parenthesis is the objective values recalculated without model reduction.

Table 4

Optimization results for the second frequency range with the adjoint variable approximation with Eq. (53).

Method		Iteration	Objective function value (m rad/s) ^a	Total cpu time (s)	Time per iter (s)
Standard method		536	1.047×10^{-4}	14,509	27.0
MS method	$n_d = 25$	600	3.2519×10^{-4} (1.0327×10^{-4})	5777	9.2
	$n_d = 50$	176	5.9040×10^{-5} (8.9948×10^{-4})	6110	10.1
RV method	$n_d = 25$	417	1.2617×10^{-4} (1.1506×10^{-4})	4737	11.3
	$n_d = 50$	600	7.2244×10^{-5} (5.8516×10^{-5})	7509	12.5
QSRV method	$n_d = 25$	600	8.668×10^{-5} (7.6718×10^{-5})	6388	10.6
	$n_d = 50$	600	8.393×10^{-5} (5.9922×10^{-5})	7939	13.2

^a The objective value in parenthesis is the objective values recalculated without model reduction.MSW $n_d = 50$ MSWO $n_d = 50$

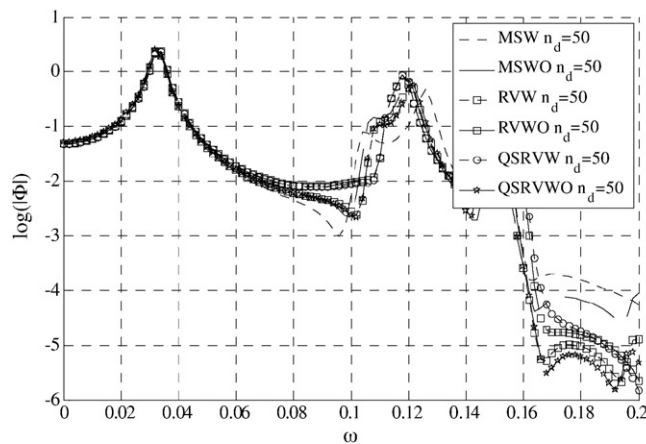
(a)

RVW $n_d = 50$ RVWO $n_d = 50$

(b)

QSRVW $n_d = 50$ QSRVWO $n_d = 50$

(c)



(d)

Fig. 23. Optimization results with the penalty $\sum \gamma(1 - \gamma)$ (a) in the MS method, (b) in the RV method, (c) in the QSRV method and (d) the frequency response curves.

proper optimization strategy should be chosen depending on the underlying optimization problem and available computational resources.

5. Conclusions

This paper discusses topology optimization using three model reduction schemes such as the mode superposition method, the Ritz vector method, the quasi-static Ritz vector method in the framework of the SIMP approach. In computational structural dynamics, numerical difficulties arise, particularly in situations where the dynamic response of a complex manifold structure is of interest in the time or frequency domains, which may make it necessary to use the MR schemes. However, these MR schemes have not been popular for use in topology optimization method. Thus this study investigated in detail the applications of these three popular MR schemes for topology optimization of dynamic system.

Each MR scheme has a distinct and unique way of constructing the reduction bases (called the generalized or modal coordinates) for approximating the structural response. The MS method uses some of the lowest eigenmodes of dynamic structure for its basis functions, whereas the RV or QSRV methods calculate its basis functions by considering external force as well as mass and stiffness matrices. Because the highly localized eigenmodes, which are locally vibrating eigen modes especially near to Void areas having weak Young's moduli, this study found that the MS method is not effective for the SIMP approach; there have been previous contributions of the MS method to the homogenization based topology optimization, and if the underlying topology optimization problem is free from these local modes such as reinforcement structure design problems, the MS method becomes effective even in the SIMP-based approach. The RV or QSRV methods were found to be free from these local mode issues. Consequently, the two MR schemes can effectively and accurately reduce the matrix size of an original dynamic system and showed good convergences in topology optimization, which is one of the main findings of this study.

Furthermore, if the underlying object or constraint function is not a self-adjoint operator, the adjoint variable should be calculated by solving the adjoint problem whose force term is a function of by the approximated structural responses. Thus, with the reduced dynamic stiffness matrix, the adjoint variable can be adversely modified compared with the structural response. Empirically it turned out that it is also possible to use the unreduced dynamic stiffness matrix, which inevitably increases the computation time, to obtain an accurate adjoint variable. Therefore, a compromise between the accuracy and efficiency of the MR schemes should be considered in real applications.

In conclusion, this study found that the MR schemes can achieve topology optimization for dynamic structures efficiently. The present research can be extended to design problems for nonlinear transient structures and wave guide design. In addition, developing a new MR scheme that combines the advantages of both modal and Ritz vectors can be useful and is a future research topic for topology optimization.

References

- [1] M.P. Bendsøe, O. Sigmund, *Topology Optimization Theory, Methods and Applications*, Springer-Verlag, New York, 2003.
- [2] G.H. Yoon, J.S. Jensen, O. Sigmund, Topology optimization of acoustic-structure interaction problems using a mixed finite element formulation, *Int. J. Numer. Methods Engrg.* 70 (2007) 1049–1076.
- [3] L.W. Lee, S.M. Wan, D. Altay, Topology optimization for the radiation and scattering of sound from thin-body using genetic algorithms, *J. Sound Vibration* 276 (2004) 899–918.
- [4] C.S. Jog, Topology design of structures subjected to periodic loading, *J. Sound Vibration* 253 (3) (2002) 687–709.
- [5] A.R. Diaz, N. Kikuchi, Solutions to shape and topology eigenvalue optimization using a homogenization method, *Int. J. Numer. Methods Engrg.* 35 (1992) 1487–1502.
- [6] G.H. Yoon, Y.Y. Kim, Optimal design of the optical pickup suspension plates using topology optimization, *Am. Inst. Aeronaut. Astronaut.* 41 (9) (2003) 1841–1843.
- [7] Z.D. Ma, N. Kikuchi, I. Hagiwara, Structural topology and shape optimization for a frequency response problem, *Comput. Mech.* 13 (3) (1993) 157–174.
- [8] Z.D. Ma, N. Kikuchi, H.C. Cheng, I. Hagiwara, Topology optimization technique for free vibration problems, *J. Appl. Mech.* 62 (1995) 200–207.
- [9] N.L. Pedersen, Maximization of eigenvalues using topology optimization, *Struct. Multidiscip. O.* 20 (1) (2000) 2–11.
- [10] T.S. Kim, Y.Y. Kim, Mac-based mode-tracking in structural topology optimization, *Comput. Struct.* 74 (2000) 375–383.
- [11] J. Du, N. Olhoff, Topological design of freely vibrating continuum structures for maximum values of simple and multiple eigenfrequencies and frequency gaps, *Struct. Multidiscip. O.* 34 (2007) 91–110.
- [12] Y. Maeda, S. Nishiwaki, K. Izui, M. Yoshimura, K. Matsui, K. Terada, Structural topology optimization of vibrating structures with specified eigenfrequencies and eigenmode shapes, *Int. J. Numer. Methods Engrg.* 67 (2006) 597–628.
- [13] G.H. Yoon, Y.Y. Kim, Element connectivity parameterization for topology optimization of geometrically nonlinear structures, *Int. J. Solids Struct.* 42 (7) (2005) 1983–2009.
- [14] G.H. Yoon, Y.Y. Kim, The element connectivity parameterization formulation for the topology design optimization of multiphysics systems, *Int. J. Numer. Methods Engrg.* 64 (2005) 1649–1677.
- [15] B.S. Kang, G.J. Park, An overview of optimization of structures subjected to transient loads, *KSME* 29 (2005) 369–386.
- [16] H.A. Lee, Y.I. Kim, G.J. Park, R.M. Kolonay, M. Blair, R.A. Canfield, Nonlinear dynamic response structural optimization of a joined-wing using equivalent static loads, *J. Aircraft* 46 (3) (2007) 821–831.
- [17] G.H. Yoon, Maximizing the fundamental eigenfrequency of geometrically nonlinear structures using the element connectivity based topology optimization, *Computers and Structures* 88 (2010) 120–133.
- [18] D. Tcherniak, Topology optimization of resonating structures using SIMP method, *Int. J. Numer. Methods Engrg.* 54 (2002) 1605–1622.
- [19] A.P. Seyranian, E. Lund, N. Olhoff, Multiple eigenvalues in structural optimization problems, *Struct. Optimization* 8 (1994) 207–227.
- [20] R.J. Guyan, Reduction of Stiffness and Mass Matrices, *AIAA J.* 3 (2) (1964) 380.
- [21] K.J. Bathe, *Finite element procedures*, Prentice hall, New Jersey, 1996.
- [22] R.D. Cook, D.S. Malkus, M.E. Plesha, R.J. Witt, *Concepts and Applications of Finite Element Analysis*, 4th Edition John Wiley & Sons, USA, 2001.
- [23] J.S. Jensen, Topology optimization of dynamics problems with Padé approximants, *Int. J. Numer. Methods Engrg.* 72 (2007) 1605–1630.
- [24] M.M. Neves, H. Rodrigues, J.M. Guedes, Generalized topology design of structures with a buckling load criterion, *Struct. Optim.* 10 (1995) 71–78.
- [25] M. Bruyneel, P. Duysinx, Note on topology optimization of continuum structures including self-weight, *Struct. Multidiscip. O.* 29 (4) (2004) 245–256.
- [26] K. Svanberg, The method of moving asymptotes – a new method for structural optimization, *Int. J. Numer. Methods Engrg.* 24 (1987) 359–373.
- [27] J. Gu, Z.D. Ma, G.M. Hulbert, A new load-dependent Ritz vector method for structural dynamics analyses: quasi-static Ritz vectors, *Finite Elem. Anal. Des.* 36 (2000) 261–278.
- [28] E.L. Wilson, A new method of dynamic analysis for linear and nonlinear systems, *Finite Elem. Anal. Des.* 1 (1985) 21–23.
- [29] J.M. Dickens, J.M. Nakagawa, M.J. Wittbrodt, A critique of mode acceleration and modal truncation augmentation methods for modal response analysis, *Comput. Struct.* 62 (1997) 985–998.
- [30] J.S. Han, M. Claas, W. Ulrike, J.G. Korvink, Design, simulation, and fabrication of a quadstable monolithic mechanism with X- and Y-directional bistable curved beams, *J. Mech. Des.* 129 (2007) 1198–1203.